Biogeosciences, 17, 3487–3510, 2020
https://doi.org/10.5194/bg-17-3487-2020

Biogeosciences Open Access EGU

Seawater pH reconstruction using boron isotopes in multiple planktonic foraminifera species with different depth habitats and their potential to constrain pH and pCO_2 gradients

Maxence Guillermic[1,2], Sambuddha Misra[3,4], Robert Eagle[1,2], Alexandra Villa[1,5], Fengming Chang[6], and Aradhna Tripati[1,2]

[1]Department of Earth, Planetary, and Space Sciences, Department of Atmospheric and Oceanic Sciences, Institute of the Environment and Sustainability, UCLA, University of California – Los Angeles, Los Angeles, CA 90095, USA
[2]Laboratoire Géosciences Océan UMR6538, UBO, Institut Universitaire Européen de la Mer, Rue Dumont d'Urville, 29280 Plouzané, France
[3]Indian Institute of Science, Centre for Earth Sciences, Bengaluru, Karnataka 560012, India
[4]The Godwin Laboratory for Palaeoclimate Research, Department of Earth Sciences, University of Cambridge, Cambridge, UK
[5]Department of Geoscience, University of Wisconsin, Madison, WI 53706, USA
[6]Key Laboratory of Marine Geology and Environment, Institute of Oceanology, Chinese Academy of Sciences, Qingdao 266071, China

Correspondence: Maxence Guillermic (maxence.guillermic@gmail.com) and Aradhna Tripati (atripati@g.ucla.edu)

Received: 3 July 2019 – Discussion started: 8 August 2019
Revised: 28 April 2020 – Accepted: 15 May 2020 – Published: 8 July 2020

Abstract. Boron isotope systematics of planktonic foraminifera from core-top sediments and culture experiments have been studied to investigate the sensitivity of $\delta^{11}B$ of calcite tests to seawater pH. However, our knowledge of the relationship between $\delta^{11}B$ and pH remains incomplete for many taxa. Thus, to expand the potential scope of application of this proxy, we report $\delta^{11}B$ data for seven different species of planktonic foraminifera from sediment core tops. We utilize a method for the measurement of small samples of foraminifera and calculate the $\delta^{11}B$-calcite sensitivity to pH for *Globigerinoides ruber*, *Trilobus sacculifer* (sacc or without sacc), *Orbulina universa*, *Pulleniatina obliquiloculata*, *Neogloboquadrina dutertrei*, *Globorotalia menardii*, and *Globorotalia tumida,* including for unstudied core tops and species. These taxa have diverse ecological preferences and are from sites that span a range of oceanographic regimes, including some that are in regions of air–sea equilibrium and others that are out of equilibrium with the atmosphere. The sensitivity of $\delta^{11}B_{carbonate}$ to $\delta^{11}B_{borate}$ (e.g., $\Delta\delta^{11}B_{carbonate}/\Delta\delta^{11}B_{borate}$) in core tops is consistent with previous studies for *T. sacculifer* and *G. ruber* and close to unity for *N. dutertrei*, *O. universa*, and combined deep-dwelling species. Deep-dwelling species closely follow the core-top calibration for *O. universa*, which is attributed to respiration-driven microenvironments likely caused by light limitation and/or symbiont–host interactions. Our data support the premise that utilizing boron isotope measurements of multiple species within a sediment core can be utilized to constrain vertical profiles of pH and pCO_2 at sites spanning different oceanic regimes, thereby constraining changes in vertical pH gradients and yielding insights into the past behavior of the oceanic carbon pumps.

1 Introduction

The oceans are absorbing a substantial fraction of anthropogenic carbon emissions, resulting in declining surface ocean pH (IPCC, 2014). Yet there is a considerable uncertainty over the magnitude of future pH change in different parts of the ocean and the response of marine biogeochemi-

cal cycles to physiochemical parameters (T, pH) caused by climate change (Bijma et al., 2002; Ries et al., 2009). Therefore, there is an increased interest in reconstructing past seawater pH (Hönisch and Hemming, 2004; Liu et al., 2009; Wei et al., 2009; Douville et al., 2010), in understanding spatial variability in aqueous pH and carbon dioxide (pCO_2) (Foster, 2008; Martínez-Boti et al., 2015b; Raitzsch et al., 2018), and in studying the response of the biological carbon pump using geochemical proxies (Yu et al., 2007, 2010, 2016).

Although all proxies for carbon cycle reconstruction are complex in nature (Pagani et al., 2005; Tripati et al., 2009, 2011; Allen and Hönisch, 2012), the boron isotope composition of foraminiferal tests (expressed as $\delta^{11}B_{carbonate}$) is emerging as one of the more robust available tools (Ni et al., 2007; Foster et al., 2008, 2012; Henehan et al., 2013; Martínez-Boti et al., 2015b; Chalk et al., 2017). The study of laboratory-cultured foraminifera has demonstrated a systematic dependence of the boron isotope composition of tests on solution pH (Sanyal et al., 1996, 2001; Henehan et al., 2013, 2016). Core-top measurements on globally distributed samples also show a boron isotope ratio sensitivity to pH with taxa-specific offsets from the theoretical fractionation line of borate ions (Rae et al., 2011; Henehan et al., 2016; Raitzsch et al., 2018).

Knowledge of seawater pH, in conjunction with constraints on one other carbonate system parameter (total alkalinity (TA), DIC (dissolved inorganic carbon), $[HCO_3^-]$, $[CO_3^{2-}]$), can be utilized to constrain aqueous pCO_2. Application of empirical calibrations for boron isotope ratio, determined for select species of foraminifera from core tops and laboratory cultures, has resulted in accurate reconstructions of pCO_2 utilizing downcore samples from sites that are currently in quasi-equilibrium with the atmosphere at present. Values of pCO_2 reconstructed from planktonic foraminifera boron isotope ratios are analytically indistinguishable from ice core CO_2 records (Foster et al., 2008; Henehan et al., 2013; Chalk et al., 2017).

The last decade has produced several studies aiming at reconstructing past seawater pH using boron isotopes to constrain atmospheric pCO_2 in order to understand the changes in the global carbon cycle (Hönisch et al., 2005, 2009; Foster et al., 2008, 2012, 2014; Seki et al., 2010; Bartoli et al., 2011; Henehan et al., 2013; Martínez-Boti et al., 2015a, b; Chalk et al., 2017). In addition to reconstructing atmospheric pCO_2, the boron isotope proxy has been applied to mixed-layer planktonic foraminifera at sites out of equilibrium with the atmosphere to constrain past air–sea fluxes (Foster et al., 2014; Martínez-Boti et al., 2015b). A small body of work has examined whether data for multiple species in core-top (Foster et al., 2008) and down-core samples could be used to constrain vertical profiles of pH through time (Palmer et al., 1998; Pearson and Palmer, 1999; Anagnostou et al., 2016).

Here we add to the emerging pool of boron isotope data in planktonic foraminifera from different oceanographic regimes, including data for species that have not previously been examined. We utilize a low-blank (15 to 65 pg B), high-precision (2 SD on the international standard JCp-1 is 0.20 ‰, $n = 6$) $\delta^{11}B_{carbonate}$ analysis method for small samples (down to $\sim 250\,\mu g$ $CaCO_3$), modified after Misra et al. (2014a), to study multiple species of planktonic foraminifera. The studied sediment core tops span a range of oceanographic regimes, including open-ocean oligotrophic settings and marginal seas. We constrain calibrations for different species, and we compare results to published work (Foster et al., 2008; Henehan et al., 2013, 2016; Martínez-Boti et al., 2015b; Raitzsch et al., 2018). We also test whether these data support the application of boron isotope measurements of multiple species within a sediment core as a proxy for constraining vertical profiles of pH and pCO_2.

2 Background

2.1 Planktonic foraminifera as archives of seawater pH

Planktonic foraminifera are used as archives of past environmental conditions within the mixed layer and thermocline, as their chemical composition is correlated with the physiochemical parameters of their calcification environment (Ravelo and Fairbanks, 1992; Elderfield and Ganssen, 2000; Dekens et al., 2002; Anand et al., 2003; Sanyal et al., 2001; Ni et al., 2007; Henehan et al., 2013, 2015, 2016; Howes et al., 2017; Raitzch et al., 2018). The utilization of geochemical data for multiple planktonic foraminifera species with different ecological preferences to constrain vertical gradients has been explored in several studies. The framework for such an approach was first developed using modern samples of planktonic foraminifera for oxygen isotopes, where it was proposed as a tool to constrain vertical temperature gradients and study physical oceanographic conditions during periods of calcification (Ravelo and Fairbanks, 1992).

Because planktonic foraminifera species complete their life cycle in a particular depth habitat due to their ecological preference (Ravelo and Fairbanks, 1992; Farmer et al., 2007), it is theoretically possible to reconstruct water column profiles of pH using boron isotope ratio data from multiple taxa (Palmer and Pearson, 1998; Anagnostou et al., 2016). The potential use of an analogous approach to reconstruct past profiles of seawater pH was first highlighted by Palmer and Pearson (1998) on Eocene samples to constrain water depth pH gradients. However, in these boron isotope-based studies, it was assumed that boron isotope offset from seawater and foraminiferal carbonate was constant, which is an assumption not supported by subsequent studies (e.g., Hönisch et al., 2003; Foster et al., 2008; Henehan et al., 2013, 2016; Raitszch et al., 2018; Rae, 2018). Furthermore, boron isotope ratio differences between foraminifera species inhabiting waters of the same pH make the acquisition of more core-top and culture data essential for applications of the proxy.

2.2 Boron systematics in seawater

Boron is a conservative element in seawater with a long residence time ($\tau_B \sim 14$ Myr) (Lemarchand et al., 2002). In seawater, boron exists as trigonal boric acid $B(OH)_3$ and tetrahedral borate ion $B(OH)_4^-$ (borate). The relative abundance of boric acid and borate ions is a function of the ambient seawater pH. At standard open-ocean conditions ($T = 25\,^\circ$C and $S = 35$), the dissociation constant of boric acid is 8.60 (Dickson, 1990), implying that boron mainly exists in the form of boric acid in seawater. The fact that the pK_B and seawater pH (e.g., ~ 8.1, NBS) values are similar implies that small changes in seawater pH will induce strong variations in the abundance of the two boron species (Fig. 1).

Boron has two stable isotopes, ^{10}B and ^{11}B, with average relative abundances of 19.9 % and 80.1 %, respectively. Variations in B isotope ratio are expressed in conventional delta (δ) notation:

$$\delta^{11}B\,(‰) = 1000 \times \left(\frac{^{11}B/^{10}B_{Sample}}{^{11}B/^{10}B_{NIST\,SRM\,951}} - 1 \right), \quad (1)$$

where positive values represent enrichment in the heavy isotope ^{11}B and negative values enrichment in the light isotope ^{10}B, relative to the standard reference material. Boron isotope values are reported versus the NIST SRM 951 boric acid standard (Cantazaro et al., 1970).

$B(OH)_3$ is enriched in ^{11}B compared to $B(OH)_4^-$ with a constant offset between the two chemical species, within the range of physiochemical variation observed in seawater, given by the fraction factor (α). The fractionation (ε) between $B(OH)_3$ and $B(OH)_4^-$ of 27.2 ± 0.6 ‰ has been empirically determined by Klochko et al. (2006) in seawater. Note that Nir et al. (2015) calculate this fractionation, using an independent method, to be 26 ± 1 ‰, which is within the analytical uncertainty of the Klochko et al. (2006) value. We use a fractionation of 27.2 ‰ determined by Klochko et al. (2006) in this study.

2.3 Boron isotopes in planktonic foraminifera calcite

Many biogenic carbonate-based geochemical proxies are affected by "vital effects" or biological fractionations (Urey et al., 1951). The $\delta^{11}B_{carbonate}$ in foraminifera exhibits species-specific offsets (see Rae et al., 2018, for review) compared to theoretical predictions for the boron isotopic composition of $B(OH)_4^-$ (expressed as $\delta^{11}B_{borate}$, $\alpha = 1.0272$; Klochko et al., 2006). As the analytical and technical aspects of boron isotope measurements have improved (Foster et al., 2008; Rae et al., 2011; Misra et al., 2014b; Lloyd et al., 2018), evidence for taxonomic differences has not been eliminated but has become increasingly apparent (Foster et al., 2008, 2016; Marschall and Foster, 2018; Henehan et al 2013, 2016; Rae et al., 2018; Raitzsch et al., 2018).

At present, culture and core-top calibrations have been published for several planktonic species including *Trilobatus sacculifer*, *Globigerinoides ruber, Globigerina bulloides, Neogloboquadrina pachyderma*, and *Orbulina universa* (Foster et al., 2008; Henehan et al., 2013, 2015; Sanyal et al., 1996, 2001). Although the boron isotopic composition of several species of foraminifera is now commonly used for reconstructing surface seawater pH, for other species, there is a lack of data constraining the sensitivity of boron isotopes in foraminiferal carbonate and borate ions in seawater.

2.4 Origin of biological fractionations in foraminifera

Perforate foraminifera are calcifying organisms that maintain a large degree of biological control over their calcification space, and thus mechanisms of biomineralization may be of significant importance in controlling the $\delta^{11}B$ of the biogenic calcite. The biomineralization of foraminifera is based on seawater vacuolization (Erez, 2003; de Nooijer et al., 2014) with parcels of seawater being isolated by an organic matrix, thereby creating a vacuole filled with seawater. Recent work has also demonstrated that even if the chemical composition of the reservoirs is modified by the organism, seawater is directly involved in the calcification process with vacuoles formed at the periphery of the shell (de Nooijer et al., 2014). Culture experiments by Rollion-Bard and Erez (2010) have proposed that the pH at the site of biomineralization is elevated to an upper pH limit of ~ 9 for the shallow-water, symbiont-bearing benthic foraminifera *Amphistegina lobifera*, which would support a pH modulation of a calcifying fluid in foraminifera. The extent to which these results apply to planktonic foraminifera is not known, although pH modulation of calcifying fluid may influence the $\delta^{11}B$ of planktonic foraminifera.

For taxa with symbionts, the microenvironment surrounding the foraminifera is chemically different from seawater due to photosynthetic activity (Jørgensen et al., 1985; Rink et al., 1998; Köhler-Rink and Kühl, 2000). Photosynthesis by symbionts elevates the pH of microenvironments (Jørgensen et al., 1985; Rink et al., 1998; Wolf-Gladrow et al., 1999; Köhler-Rink and Kühl, 2000), while calcification and respiration decrease microenvironment pH (Eqs. 2 and 3).

$$Ca^{2+} + 2HCO_3^- \leftrightarrow CaCO_3 + H_2O + CO_2 \text{ or}$$
$$Ca^{2+} + CO_3^{2-} \leftrightarrow CaCO_3 \quad \text{[calcification]} \quad (2)$$
$$CH_2O + O_2 \leftrightarrow CO_2 + H_2O \quad \text{[respiration/photosynthesis]} \quad (3)$$

$\delta^{11}B$ in foraminifera is primarily controlled by seawater pH but also depends on the pH alteration of microenvironments due to calcification, respiration, and symbiont photosynthesis. $\delta^{11}B_{carbonate}$ should therefore reflect the relative dominance of these processes and may account for species-specific $\delta^{11}B$ offsets. Theoretical predictions from Zeebe et al. (2003) and foraminiferal data from Hönisch et al. (2003) explored the influence of microenvironment pH in the $\delta^{11}B$ signature of foraminifera. Their work also suggested that for a given species there should be a constant offset observed

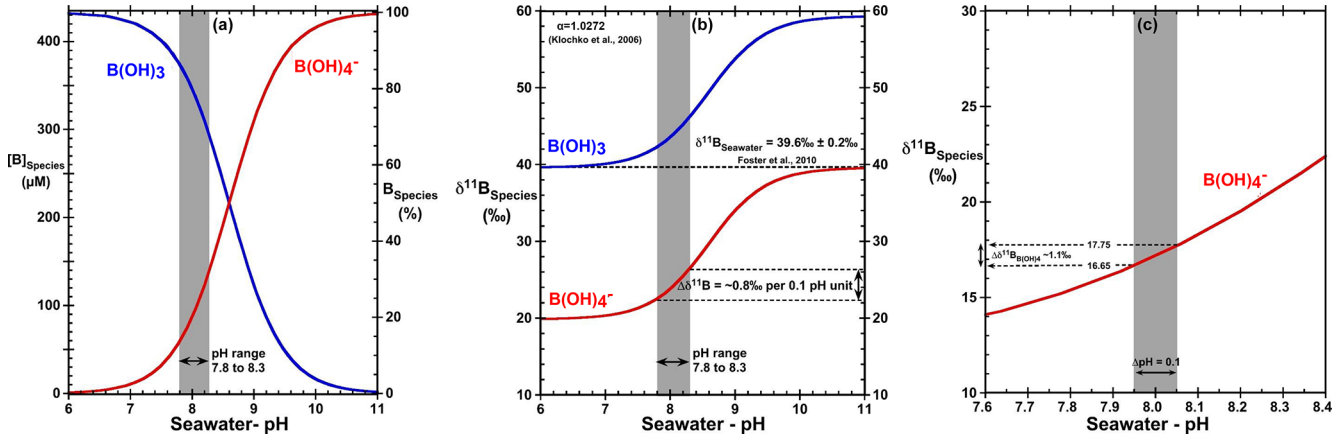

Figure 1. (a) Speciation of $B(OH)_3$ and $B(OH)_4^-$ as a function of seawater pH (total scale), **(b)** $\delta^{11}B$ of dissolved inorganic boron species as a function of seawater pH, **(c)** sensitivity of $\delta^{11}B$ of $B(OH)_4^-$ for a pH ranging from 7.6 to 8.4. $T = 25\,°C$, $S = 35$, $\delta^{11}B = 39.61\,‰$ (Foster et al., 2010), and dissociation constant $\alpha = 1.0272$ (Klochko et al., 2006).

between the boron isotope composition of foraminifera and borate ions over a large range of pH, imparting confidence in utilizing species-specific boron isotope data as a proxy for seawater pH.

Comparison of boron isotope data for multiple planktonic foraminiferal species indicates that taxa with high levels of symbiont activity such as *T. sacculifer* and *G. ruber* show higher $\delta^{11}B$ values than the $\delta^{11}B$ of ambient borate (Foster et al., 2008; Henehan et al., 2013; Raitzsch et al., 2018). The sensitivities $\Delta\delta^{11}B_{carbonate}/\Delta\delta^{11}B_{borate}$ (hereafter referred to as the slope) of existing calibrations suggest a different species-specific sensitivity for these species compared to other taxa (Sanyal et al., 2001; Henehan et al., 2013, 2015; Raitzsch et al., 2018). For example, *Orbulina universa* exhibits a lower $\delta^{11}B$ than in situ $\delta^{11}B$ values of borate ions (Henehan et al., 2016), consistent with the species living deeper in the water column characterized by reduced photosynthetic activity.

It is possible that photosynthetic activity by symbionts might not be able to compensate for changes in calcification and/or respiration, leading to an acidification of the microenvironment. It is interesting to note that for *O. universa* the slope determined for the field-collected samples is not statistically different from unity (0.95 ± 0.17) (Henehan et al., 2016), while culture experiments report slopes of ≤ 1 for multiple species including *G. ruber* (Henehan et al., 2013), *T. sacculifer* (Sanyal et al., 2001), and *O. universa* (Sanyal et al., 1999). More core-top and culture calibrations are needed to refine those slopes and understand if significant differences are observed, which is part of the motivation for this study.

2.5 Planktic foraminifera depth and habitat preferences

The preferred depth habitat of different species of planktonic foraminifera depends on their ecology, which in turn is dependent on hydrographic conditions. For example, *G. ruber is* commonly found in the mixed layer (Fairbanks and Wiebe, 1980; Dekens et al., 2002; Farmer et al., 2007) during the summer (Deuser et al., 1981), whereas *T. sacculifer* is present in the mixed layer until mid-thermocline depths (Farmer et al., 2007) during spring and summer (Deuser et al., 1981, 1989). Specimens of *P. obliquiloculata* and *N. dutertrei* are abundant during winter months (Deuser et al., 1989), with an acme in the mixed layer (~ 60 m) for *P. obliquiloculata* and at mid-thermocline depths for *N. dutertrei* (Farmer et al., 2007). In contrast, *O. universa* tends to record annual average conditions within the mixed layer. Specimens of *G. menardii* calcify within the seasonal thermocline (Fairbanks et al., 1982; Farmer et al., 2007; Regenberg et al., 2009), and in some regions in the upper thermocline (Farmer et al., 2007), and record annual temperatures. *G. tumida* is found at the lower thermocline or below the thermocline and records annual average conditions (Fairbanks and Wiebe, 1980; Farmer et al., 2007; Birch et al., 2013). Although the studies listed above showed evidence for species-specific living depth habitat affinities, recent direct observations showed that environmental conditions (e.g., temperature, light) were locally responsible for the variability in the living depth of certain foraminifera species in the eastern North Atlantic (Rebotim et al., 2017).

Table 1. Box core information.

Label	Box core	Site	Latitude (N)	Longitude (E)	Depth (m b.s.l.)	Oceanic regime	^{14}C age (year)
Atlantic Ocean							
CD107-a	CD107	A	52.92	−16.92	3569	non-upwelling	<3000[a]
Indian Ocean							
FC-01a	WIND-33B	I	−11.21	58.77	3520	non-upwelling	
FC-02a	WIND-10B	K	−29.12	47.55	2871	non-upwelling	7252 ± 27[b]
Arabian Sea							
FC-12b	CD145	A150	23.30	66.70	151	seasonal upwelling	
FC-13a	CD145	A3200	20.00	65.58	3190	seasonal upwelling	
Pacific Ocean							
WP07-01			−3.93	156.00	1800	non-upwelling	7300–8600[c]
A14			8.02	113.39	1911	non-upwelling	7300–8600[c]
806		A	0.32	159.36	2521	equatorial divergence	7300–8600[c]
807		A	3.61	156.62	2804	equatorial divergence	7300–8600[c]

[a] Thomson et al., 2000. [b] Wilson et al., 2012. [c] Age for core top of site 806B from Lea et al. (2000).

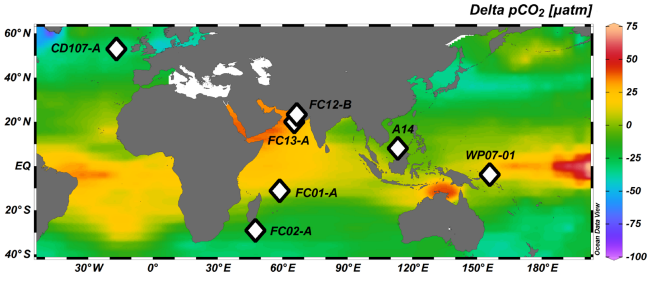

Figure 2. Map showing locations of the core tops used in this study (white diamonds). Red open circles represent the sites used for in situ carbonate parameters from the GLODAP database (Key et al., 2004).

3 Materials and methods

3.1 Localities studied

Core-top locations were selected to span a broad range of seawater pH, carbonate system parameters, and oceanic regimes. Samples from the Atlantic Ocean (CD107-A), Indian Ocean (FC-01a and FC-02a), Arabian Sea (FC-13a and FC-12b), and Pacific Ocean (WP07-01, A14, and Ocean Drilling Program 806A and 807A) were analyzed; characteristics of the sites are summarized in Tables 1 and S7 and Figs. 2 and 3.

Atlantic site CD107-a (CD107 site A) was cored in 1997 by the Benthic Boundary Layer program (BENBO) (Black, 1997 – cruise report RRS *Charles Darwin* cruise 107). Arabian Sea sites FC-12b (CD145 A150) and FC-13a (CD145 A3200) were retrieved by the *Charles Darwin* in the Pakistan margin in 2004 (Bett, 2004 – cruise report no. 50 RRS *Charles Darwin* cruise 145). A14 was recovered by a box corer in the southern area of the South China Sea in 2012. Core WP07-01 was obtained from the Ontong Java Plateau using a giant piston corer during the Warm Pool Subject Cruise in 1993. Holes 806A and 807A were retrieved on Leg 130 by the Ocean Drilling Program (ODP). The top 10 cm of sediment from CD107-A has been radiocarbon dated to be Holocene <3 kyr (Thomson et al., 2000). Samples from multiple box cores from Indian Ocean sites were radiocarbon dated as Holocene <7.3 kyr (Wilson et al., 2012). Samples from western equatorial Pacific site 806B, close to site WP07-01, are dated to between 7.3 and 8.6 kyr (Lea et al., 2000). Arabian Sea and Pacific core-top samples were not radiocarbon dated but are assumed to be Holocene.

3.2 Species

Around 50–100 foraminifera shells were picked from the 400 to 500 µm fraction size for *Globorotalia menardii* and *Globorotalia tumida*, >500 µm for *Orbulina universa*, and from the 250–400 µm fraction size for *Trilobatus sacculifer* (w/o sacc, without sacc-like final chamber), *Trilobatus sacculifer* (sacc, sacc-like final chamber), *Globigerinoides ruber* (white, sensu stricto), *Neogloboquadrina dutertrei*, and *Pulleniatina obliquiloculata*. The samples picked for analyses were visually well preserved.

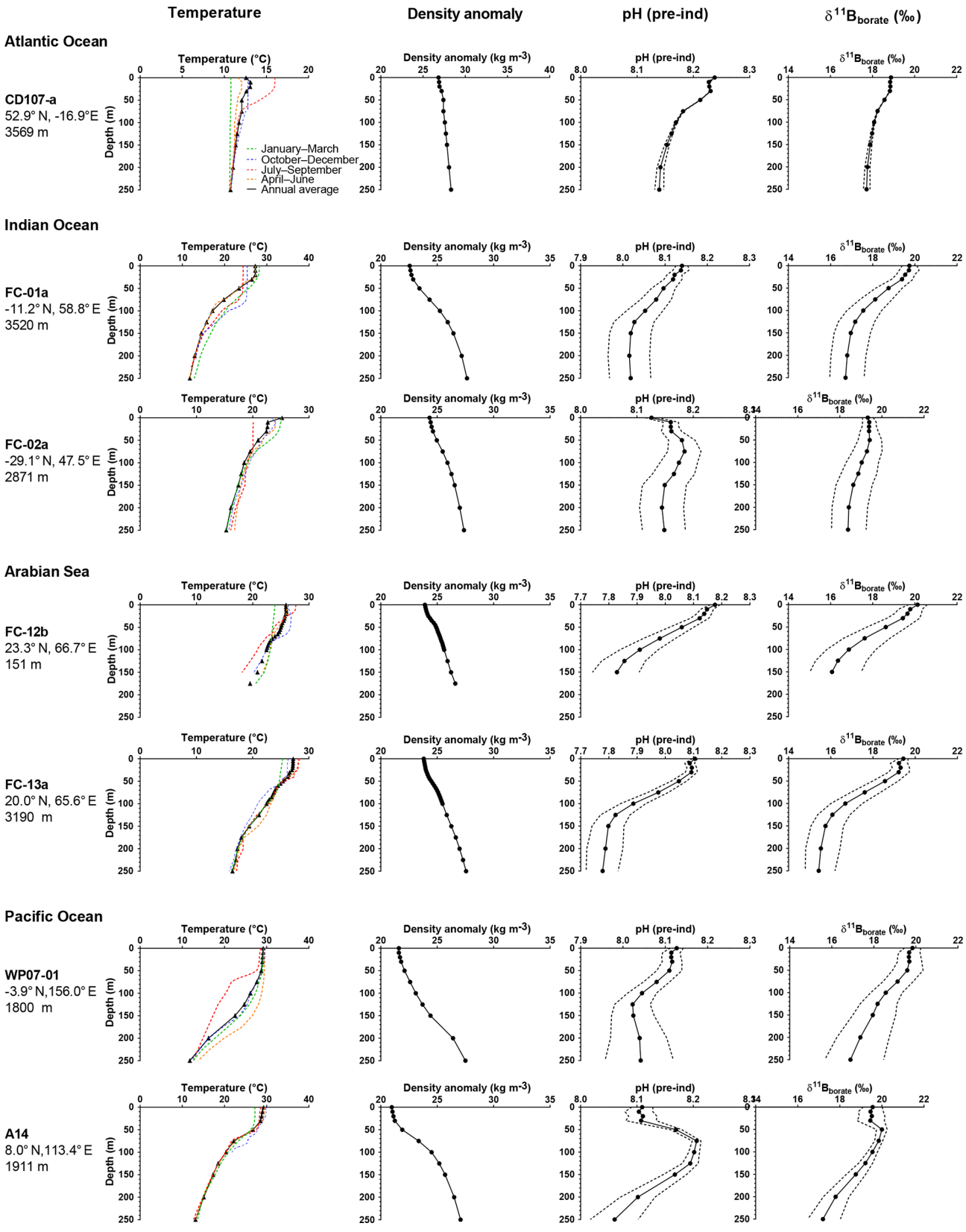

Figure 3. Preindustrial data versus depth for the sites used in this study. The figure shows seasonal temperatures (extracted from World Ocean Database 2013), density anomaly (kg m^{-3}), and preindustrial pH and preindustrial $\delta^{11}B$ of $H_4BO_4^-$ (calculated from the GLODAP database and corrected for anthropogenic inputs). Dotted lines are the calculated uncertainties based on errors on TA and DIC from the GLODAP database.

3.3 Sample cleaning

Briefly, picked foraminifera were gently cracked open, clay was removed with successive ultrasonication steps in MQ water and methanol, and then they were checked for coarse-grained silicates. The next stages of sample processing and chemical separation were performed in a class 1000 clean lab equipped with boron-free HEPA filters. Samples were cleaned using full reductive and oxidative cleaning (Boyle, 1981; Boyle and Keigwin, 1985; Barker et al., 2003). Samples from the South China Sea (sites A14, E035) presented high Mn and high Fe. Due to potential Fe-Mn oxide and hydroxides the reductive cleaning was used. Previous comparisons of cleaning methods have shown there is no impact of the reductive step on B/Ca (Misra et al., 2014b), but there is an impact of the reductive step on Mg/Ca (Barker et al., 2003 and others). Nevertheless, it is possible that Fe-Mn oxide and hydroxides can result in non-negligible Mg and B contamination. Because this study was designed to investigate boron proxies and in order to be consistent in methodology, the reductive cleaning was used at all sites. Cleaned samples selected for this study did not yield high Mn concentrations (see Supplement for discussion on contamination).

A final leaching step with 0.001 N HCl was done before dissolution in 1 N HCl. Hydrochloric acid was used to allow complete dissolution of the sample including Fe-Mn oxide and hydroxides if present. Each sample was divided into two aliquots: an aliquot for boron purification and one aliquot for trace element analysis.

3.4 Reagents

Double-distilled HNO_3 and HCl acids (from Merck® grade) and a commercial bottle of ultrapure-grade HF were used at Brest. Double-distilled acids were used at Cambridge. All acids and further dilutions were prepared using double-distilled 18.2 MΩ cm^{-1} MQ water. Working standards for isotope ratio and trace element measurements were freshly diluted on a daily basis with the same acids used for sample preparation to avoid any matrix effects.

3.5 Boron isotopes

Boron purification for isotopic measurement was done utilizing the microdistillation method developed by Gaillardet et al. (2001) for Ca-rich matrices by Wang et al. (2010) and adapted at Cambridge by Misra et al. (2014a). A total of 70 µL of carbonate sample dissolved in 1 N HCl was loaded on a cap of a clean fin legged 5 mL conical beaker upside down. The tightly closed beaker was put on a hot plate at 95 °C for 15 h. The beakers were taken off the hot plate and were allowed to cool for 15 min. The cap where the residue formed was replaced by a clean one. Then, 100 µL of 0.5 % HF was added to the distillate.

Boron isotopic measurements were carried out on a Thermo Scientific® Neptune+ MC-ICP-MS at the University of Cambridge. The Neptune+ was equipped with a Jet interface and two $10^{13}\Omega$ resistors. The instrumental setup included Savillex® 50 µL min^{-1} C-flow self-aspirating nebulizer, a single-pass Teflon® Scott-type spray chamber constructed utilizing Savillex® column components, a 2.0 mm Pt injector from ESI®, a Thermo® Ni "normal"-type sample cone, and 'X' type skimmer cones. Both isotopes of boron were determined utilizing $10^{13}\Omega$ resistors (Misra et al., 2014a; Lloyd et al., 2018).

The sample size for boron isotope analyses typically ranged from 10 ppb B (∼ 5 ng B) to 20 ppb B samples (∼ 10 ng B). Instrumental sensitivity for ^{11}B was 17 mV ppb^{-1} B (e.g., 170 mV for 10 ppb B) in wet plasma at a 50 µL min^{-2} sample aspiration rate. Intensity of ^{11}B for a sample at 10 ppb B was typically 165 mV ± 5 mV, which closely matched the 170 mV ± 5 mV of the standard. Due to the low boron content of the samples, extreme care was taken to avoid boron contamination during sample preparation and reduce memory effect during analysis. Procedural boron blanks ranged from 15 to 65 pg B and contributed to less than <1 % of the sample signal. The acid blank during analyses was measured at ≤ 1 mV on ^{11}B, meaning a contribution <1 % of the sample intensity; no memory effect was observed within and across sessions. No matrix effect resulting from the mix HCl/HF was observed on the δ^{11}B.

Analyses of external standards were done to ensure data quality. For δ^{11}B measurements one carbonate standard and one coral were utilized: the JCp-1 (Geological Survey of Japan, Tsukuba, Japan) international standard (Gutjahr et al., 2014) and the NEP coral (*Porites* sp., $\delta^{11}B = 26.12 \pm 0.92$ ‰, 2SD, $n = 33$, Holcomb et al., 2015, and Sutton et al., 2018, Table S2 in the Supplement) from University of Western Australia–Australian National University. A certified boric acid standard, the ERM© AE121 ($\delta^{11}B = 19.9 \pm 0.6$ ‰, SD, certified), was used to monitor reproducibility and drift during each session (Vogl and Rosner, 2011; Foster et al., 2013; Misra et al., 2014b). Results for the isotopic composition of the NEP coral are shown in Table S2, average values are $\delta^{11}B_{NEP} = 25.70 \pm 0.93$ ‰ (2SD, $n = 22$) over seven different analytical sessions with each number representing an ab initio processed sample. Our results are within error of published values of 26.20 ± 0.88 ‰ (2SD, $n = 27$) and 25.80 ± 0.89 ‰ (2SD, $n = 6$) by Holcomb et al. (2015) and Sutton et al. (2018), respectively. Chemically cleaned JCp-1 samples were measured at 24.06 ± 0.20 (2SD, $n = 6$) and are within error of published values of 24.37 ± 0.32 ‰, 24.11 ± 0.43 ‰, and 24.42 ± 0.28 ‰ by Holcomb et al. (2015), Farmer et al. (2016), and Sutton et al. (2018), respectively.

3.6 Trace elements

The calcium concentration of each sample was measured on an inductively coupled plasma atomic emission spectrome-

ter (ICP-AES) Ultima 2 HORIBA at the Pôle spectrometrie Océan (PSO), UMR6538 (Plouzané, France). Samples were then diluted to fixed calcium concentrations (typically 10 ppm or 30 ppm Ca) using 0.1 M HNO_3 and 0.3 M HF matching multielement standard Ca concentration to avoid any matrix effects (Misra et al., 2014b). Levels of remaining HCl (<1 %) in these diluted samples were negligible and did not contribute to matrix effects. Trace elements (e.g., X/Ca ratios) were analyzed on a Thermo Scientific® Element XR high-resolution inductively coupled plasma mass spectrometer (HR-ICP-MS) at the PSO, Ifremer (Plouzané, France).

Trace element analyses were done at a Ca concentration of 10 or 30 ppm. The typical blanks for a 30 ppm Ca session were ^{7}Li <2 %, ^{11}B <7 %, ^{25}Mg <0.2 %, and ^{43}Ca <0.02 %. Additionally, blanks for a 10 ppm Ca session were ^{7}Li <2.5 %, ^{11}B <10 %, ^{25}Mg <0.4 %, and ^{43}Ca <0.05 %. Due to strong memory effect for boron and instrumental drift on the Element XR, long sessions of conditioning were done prior to analyses. Boron blanks were driven below 5 % of signal intensity usually after 4 to 5 d of continuous analyses of carbonate samples. External reproducibility was determined on the consistency standard Cam-Wuellestorfi (courtesy of the University of Cambridge) (Misra et al., 2014b), Table S3. Our X/Ca ratio measurements on the external standard Cam-Wuellestorfi were within error of the published value all the time (Table S3), validating the robustness of our trace element data. Analytical uncertainty of a single measurement was calculated from the reproducibility of the Cam-Wuellestorfi, measured during a particular mass spectrometry session. The analytical uncertainties (2SD, $n = 31$, Table S3) on the X/Ca ratios are ± 0.4 µmol mol^{-1} for Li/Ca, ± 7 µmol mol^{-1} for B/Ca, and ± 0.01 µmol mol^{-1} for Mg/Ca, respectively.

3.7 Oxygen isotopes

Carbonate δ^{13}C and δ^{18}O were measured on a GasBench II coupled to a Delta V mass spectrometer at the stable isotope facility of Pôle spectrometrie Océan (PSO), Plouzané. Around 20 shells were weighed, crushed, and had clay removed following the same method described in Sect. 3.3 (Barker et al., 2003). The recovered foraminifera were weighed in tubes and flushed with He gas. Samples were then digested in phosphoric acid and analyzed. Results were calibrated to the Vienna Pee Dee Belemnite (VPDB) scale by international standard NBS19, and analytical precision on the in-house standard Ca21 was better than ± 0.11 ‰ for δ^{18}O (SD, $n = 5$) and ± 0.03 ‰ for δ^{13}C (SD, $n = 5$).

3.8 Calcification depth determination

We utilized two different chemo-stratigraphic methods to estimate the calcification depth (CD) in this study (Tables S6 and S7). The first method (CD1), commonly used in paleoceanography, utilizes δ^{18}O measurements of the carbonate ($\delta^{18}O_c$) to estimate calcification depths (referred to as δ^{18}O-based calcification depths) (Schmidt et al., 2002; Mortyn et al., 2003; Sime et al., 2005; Farmer et al., 2007; Birch et al., 2013). Rebotim et al. (2017) also showed good correspondence between living depth habitat and calcification depth derived using CD1. The second method (CD2) utilizes Mg/Ca-based temperature estimates ($T_{Mg/Ca}$) to constrain calcification depths (Quintana Krupinski et al., 2017). However, we note that reductive cleaning leads to a decrease in Mg/Ca that in turn would result in a bias towards deeper calcification depths, which is not the case when we utilize non-Mg/Ca-based methodologies. In both cases, the prerequisite was that vertical profiles of seawater temperature are available for different seasons in ocean atlases and cruise reports and that hydrographic data and geochemical proxy signatures can be compared to assess the depth in the water column that represents the taxon's maximum abundance.

Because both methods have their uncertainties (in one case use of taxon-specific calibrations and in the other analytical limitations), both estimates of calcification depth were compared to published values for the basin (CD3) and where available for the same site (Table S6). To select which calcification depth to use for further calculations, we first looked at CD_1, CD_2, and CD_3. If CD1 and CD2 were similar we selected this calcification depth, and if CD_1 and CD_2 were different we chose literature values, CD_3, when available. For some less studied species, like *G. tumida*, *G. menardii*, or *P. obliquiloculata*, CD_3 was not always available but when available showed good correspondence with our CD_2. Moreover due to availability of Mg/Ca-derived temperature taxon-specific calibrations, we preferentially use CD_2 for those species.

We applied (based on uncertainties of our measurements) an uncertainty of ± 10 m for calcification depths >70 m and an uncertainty of ± 20 m when calcification depths <70 m. Direct observations of living depths of foraminifera remain limited. However, the depth uncertainties reported here are in line with the uncertainties calculated based on direct observations in the eastern North Atlantic which give a standard error on average living depths ranging from 6 to 22 m for the same species (Rebotim et al., 2017). The decrease in Mg/Ca due to reductive cleaning was not taken into account because it has not been studied for most of the species used in this study and because the depth uncertainty applied based on δ^{18}O analytical error is conservative relative to the uncertainty of a 10 % decrease in Mg/Ca equivalent that would be equivalent to ~ 1.2 °C. The depth habitats utilized to derive in situ parameters are summarized in Table S7.

3.9 $\delta^{11}B_{borate}$

Two carbonate system parameters are needed to fully constrain the carbonate system. Following the approach of Foster et al. (2008), we used the GLODAP database (Key et al., 2004) corrected for anthropogenic inputs in order to esti-

mate preindustrial carbonate system parameters at each site. Temperature, salinity, and pressure for each site are from the World Ocean Database 2013 (Boyer et al., 2013). We utilized the R© code in Henehan et al. (2016) (courtesy of Michael Henehan) to calculate the $\delta^{11}B_{borate}$ and $\delta^{11}B_{borate}$ uncertainty and derive our calibrations. Uncertainty for $\delta^{11}B_{borate}$ utilizing Henehan's code was similar to uncertainty calculated by applying 2SD of the $\delta^{11}B_{borate}$ profiles within the limits imposed by our calcification depth.

The MATLAB© template provided by Zeebe and Wolf-Gladow (2001) was used to calculate pCO_2 from TA; temperature, salinity, and pressure were included in the calculations. Total boron was calculated from Lee et al. (2010), and K_1 and K_2 were calculated from Mehrbach et al. (1973) refitted by Dickson and Millero (1987).

Statistical tests were performed utilizing GraphPad© software, and linear regressions for calibration were derived utilizing R© code in Henehan et al. (2016) (courtesy of Michael Henehan) with k (number of wild bootstrap replicates) equal to 500.

4 Results

4.1 Depth habitat

The calcification depths utilized in this paper are summarized in Tables S6 and S7, including a comparison of calcification depth determination methods. The calculated calcification depths are consistent with the ecology of each species and the physical properties of the water column of the sites. Specimens of *G. ruber* and *T. sacculifer* appear to be living in the shallow mixed layer (0–100 m), with *T. sacculifer* living or migrating deeper than *G. ruber* (down to 125 m). Specimens of *O. universa* and *P. obliquiloculata* are living in the upper thermocline; *G. menardii* is found in the upper thermocline until the thermocline depth specific to the location; *N. dutertrei* is living near thermocline depths and *G. tumida* is found in the lower thermocline.

Data from the multiple approaches for calculating calcification depth (CD1, CD2, and CD3) imply that some species inhabit deeper environments in the western equatorial Pacific (WEP) relative to the Arabian Sea, which in turn are deeper-dwelling than the same morphospecies occurring in the Indian Ocean. In some cases, we find evidence for differences in habitat depth of up to $\sim$ 100 m between the WEP and the Arabian Sea. This trend is observed for *G. ruber* and *T. sacculifer*, but not for *O. universa*.

Some differences are observed between the two methods for calcification depth determination that are based on $\delta^{18}O$ and Mg/Ca (CD1 and CD2). These differences might be due to the choice of calibration. Alternatively, our uncertainties for $\delta^{18}O$ imply larger uncertainties on calcification depth determinations that use this approach, compared to Mg/Ca-based estimates.

4.2 Empirical calibrations of foraminiferal $\delta^{11}B_{carbonate}$ to $\delta^{11}B_{borate}$

Results for the different species analyzed in this study are presented in Figs. 4 and 5 and summarized in Table 2; additionally, published calibrations for comparison are summarized in Table 3.

4.2.1 *G. ruber*

Samples were picked from the 250–300 µm fraction, except for the WEP sites where *G. ruber* shells were picked from the 250–400 µm fraction. Weight per shell averaged 11 ± 4 µg ($n = 4$, SD), although the weight was not measured on the same subsample analyzed for $\delta^{11}B$ and trace elements or at the WEP sites. In comparison to literature, the size fraction used for this study was smaller: Foster et al. (2008) used the 300–355 µm fraction, Henehan et al. (2013) utilized multiple size fractions (250–300, 250–355, 300–355, 355–400, and 400–455 µm), and Raitzsch et al. (2018) used the 315–355 µm fraction.

Our results for *G. ruber* (Fig. 4) are in close agreement with published data from other core tops, sediment traps, tows, and culture experiments for $\delta^{11}B_{borate} > 19$ ‰ (Foster et al., 2008; Henehan et al., 2013; Raitzsch et al., 2018). However, the two data points from $\delta^{11}B_{borate} < 19$ ‰ are lower compared to previous studies. Elevated $\delta^{11}B_{carbonate}$ values relative to $\delta^{11}B_{borate}$ have been explained by the high photosynthetic activity of symbionts (Hönisch et al., 2003; Zeebe et al., 2003). Three calibrations have been derived (Table 3). Linear regression on our data alone yields a slope of 1.12 ($\pm$1.67). The uncertainty is significant given limited data in our study, and given this large uncertainty, our sensitivity of $\delta^{11}B_{carbonate}$ to $\delta^{11}B_{borate}$ is also consistent with the low sensitivity trend of culture experiments from Sanyal et al. (2001) or Henehan et al. (2013). The second calibration made compiling all data from literature shows a sensitivity similar (e.g., 0.46 ($\pm$0.34)) to the one recently published by Raitzsch et al. (2018) (e.g., 0.45 ($\pm$0.16), Table 3). The third linear regression made only on data from the 250–400 µm fraction from our study and from the 250–300 µm fraction from Henehan et al. (2013) yields a sensitivity of 0.58 ($\pm$0.91) similar to culture experiments from Henehan et al. (2013) (e.g., 0.6 ($\pm$0.16), Table 3). This third calibration is offset by ~ -0.4 ‰ ($p > 0.05$) compared to culture calibration from Henehan et al. (2013).

4.2.2 *T. sacculifer*

$\delta^{11}B_{carbonate}$ results for *T. sacculifer* (sacc and without sacc) (Fig. 4) are compared to published data (Foster et al., 2008; Martínez-Boti et al., 2015b; Raitzsch et al., 2018). Results for *T. sacculifer* are in good agreement with the literature and exhibit higher $\delta^{11}B_{carbonate}$ compared to expected $\delta^{11}B_{borate}$ at their collection location. A linear regression through our data

https://doi.org/10.5194/bg-17-3487-2020

Table 2. Analytical results of $\delta^{13}C$, $\delta^{18}O$, and $\delta^{11}B$ and elemental ratios Li/Ca, B/Ca, and Mg/Ca.

Core	Species	Fraction size (µm)	$\delta^{13}C^a$ (‰)	$\delta^{18}O^a$ (‰)	$\delta^{11}Bc_1$ (‰)	$\delta^{11}Bc_2$ (‰)	$\delta^{11}B^b_{average}$ (µmol mol^{-1})	Li/Ca^c (µmol mol^{-1})	B/Ca^c (mmol mol^{-1})	Mg/Ca^c (µmol mol^{-1})	Mn/Ca^c (mmol mol^{-1})	Fe/Ca^c
Atlantic Ocean												
CD107a	*O. universa*	>500	1.99 ± 0.03	1.25 ± 0.11	16.85 ± 0.31 (2SD, nAE121 = 11)	16.95 ± 0.31 (2SD, nAE121 = 11)	16.90 ± 0.22	13.9 ± 0.4	68 ± 7	3.60 ± 0.01	13 ± 7	0.16 ± 0.01
Indian Ocean												
FC-01a	*G. ruber* (white ss)	250–300	1.37 ± 0.03	−1.32 ± 0.11	19.33 ± 0.31 (2SD, nAE121 = 11)	19.41 ± 0.31 (2SD, nAE121 = 11)	19.37 ± 0.22	15.4 ± 0.4	109 ± 7	3.98 ± 0.01	10 ± 7	0.07 ± 0.01
FC-01a	*T. sacculifer* (sacc)	300–400	1.88 ± 0.03	−2.20 ± 0.11	18.71 ± 0.24 (2SD, nAE121 = 10)	18.73 ± 0.24 (2SD, nAE121 = 10)	18.72 ± 0.17	12.1 ± 0.4	87 ± 7	3.45 ± 0.01	9 ± 7	0.03 ± 0.01
FC-01a	*T. sacculifer* (without sacc)	300–400	2.02 ± 0.03	−1.05 ± 0.11	19.13 ± 0.24 (2SD, nAE121 = 10)	19.32 ± 0.24 (2SD, nAE121 = 10)	19.23 ± 0.17	12.1 ± 0.4	82 ± 7	3.42 ± 0.01	14 ± 7	0.03 ± 0.01
FC-01a	*O. universa*	>500			15.50 ± 0.26 (2SD, nAE121=14)		15.50 ± 0.26					
FC-01a	*P. obliquiloculata*	300–400	1.00 ± 0.03	−0.55 ± 0.11	16.40 ± 0.26 (2SD, nAE121 = 14)	16.10 ± 0.26 (2SD, nAE121 = 14)	16.25 ± 0.18	15.4 ± 0.4	78 ± 7	2.06 ± 0.01	14 ± 7	0.05 ± 0.01
FC-01a	*G. menardii*	300–400	1.64 ± 0.03	0.43 ± 0.11	17.52 ± 0.26 (2SD, nAE121 = 14)	17.69 ± 0.26 (2SD, nAE121 = 14)	17.60 ± 0.18	12.7 ± 0.4	63 ± 7	2.26 ± 0.01	8 ± 7	0.07 ± 0.01
FC-01a	*N. dutertrei*	300–400	1.28 ± 0.03	−0.43 ± 0.11	16.40 ± 0.31 (2SD, nAE121 = 11)	16.59 ± 0.31 (2SD, nAE121 = 11)	16.50 ± 0.22	18.6 ± 0.4	73 ± 7	1.81 ± 0.01	11 ± 7	0.03 ± 0.01
FC-01a	*G. tumida*	300–400	1.29 ± 0.03	−0.53 ± 0.11	16.21 ± 0.31 (2SD, nAE121 = 11)	16.18 ± 0.31 (2SD, nAE121 = 11)	16.20 ± 0.22	10.0 ± 0.4	61 ± 7	1.79 ± 0.01	11 ± 7	0.02 ± 0.01
FC-02a	*G. ruber (white ss)*	250–300	0.30 ± 0.03	−1.40 ± 0.11	20.02 ± 0.24 (2SD, nAE121 = 10)	19.90 ± 0.24 (2SD, nAE121 = 10)	19.96 ± 0.17	18.2 ± 0.4	125 ± 7	3.47 ± 0.01	10 ± 7	0.07 ± 0.01
FC-02a	*T. sacculifer (sacc)*	300–400	1.43 ± 0.03	−1.60 ± 0.11	20.07 ± 0.24 (2SD, nAE121 = 10)	19.93 ± 0.24 (2SD, nAE121 = 10)	20.00 ± 0.17	14.2 ± 0.4	106 ± 7	3.30 ± 0.01	10 ± 7	0.03 ± 0.01
FC-02a	*O. universa*	>500	1.79 ± 0.03	0.02 ± 0.11	18.05 ± 0.26 (2SD, nAE121 = 14)	17.97 ± 0.26 (2SD, nAE121 = 14)	18.01 ± 0.18	14.8 ± 0.4	67 ± 7	4.40 ± 0.01	11 ± 7	0.05 ± 0.01
FC-02a	*P. obliquiloculata*	300–400	0.34 ± 0.03	0.56 ± 0.11	16.35 ± 0.26 (2SD, nAE121 = 14)	16.69 ± 0.26 (2SD, nAE121 = 14)	16.52 ± 0.18	16.6 ± 0.4	83 ± 7	2.33 ± 0.01	7 ± 7	0.03 ± 0.01
FC-02a	*G. menardii*	300–400	1.73 ± 0.03	−0.51 ± 0.11	17.77 ± 0.26 (2SD, nAE121 = 14)		17.77 ± 0.26	15.8 ± 0.4	125 ± 7	2.21 ± 0.01	17 ± 7	0.03 ± 0.01
FC-02a	*N. dutertrei*	300–400	1.03 ± 0.03	−0.55 ± 0.11	16.78 ± 0.31 (2SD, nAE121 = 11)	17.03 ± 0.31 (2SD, nAE121 = 11)	16.91 ± 0.22	18.6 ± 0.4	82 ± 7	2.13 ± 0.01	13 ± 7	0.07 ± 0.01
FC-02a	*G. tumida*	300–400	1.64 ± 0.03	−0.28 ± 0.11	16.93 ± 0.26 (2SD, nAE121 = 14)	16.95 ± 0.26 (2SD, nAE121 = 14)	16.94 ± 0.18	15.6 ± 0.4	87 ± 7	1.90 ± 0.01	17 ± 7	0.04 ± 0.01
Arabian Sea												
FC-12b	*G. ruber* (white ss)	250–300	0.58 ± 0.03	−2.82 ± 0.11	21.30 ± 0.31 (2SD, nAE121 = 11)	21.23 ± 0.31 (2SD, nAE121 = 11)	21.26 ± 0.22	19.5 ± 0.4	164 ± 7	5.76 ± 0.01	14 ± 7	0.16 ± 0.01
FC-12b	*T. sacculifer* (sacc)	300–400	1.76 ± 0.03	−2.15 ± 0.11	19.65 ± 0.31 (2SD, nAE121 = 11)	19.57 ± 0.31 (2SD, nAE121 = 11)	19.61 ± 0.22	14.6 ± 0.4	101 ± 7	4.28 ± 0.01	17 ± 7	0.14 ± 0.01
FC-12b	*T. sacculifer* (without sacc)	300–400	1.97 ± 0.03	−2.19 ± 0.11	20.32 ± 0.31 (2SD, nAE121 = 11)	20.37 ± 0.31 (2SD, nAE121 = 11)	20.34 ± 0.22	16.7 ± 0.4	116 ± 7	4.90 ± 0.01	20 ± 7	0.26 ± 0.01
FC-12b	*O. universa*	>500	1.89 ± 0.03	−1.59 ± 0.11	18.13 ± 0.20 (2SD, nAE121 = 6)		18.13 ± 0.20	13.6 ± 0.4	103 ± 7	6.91 ± 0.01	10 ± 7	0.06 ± 0.01
FC-12b	*P. obliquiloculata*	300–400	0.5 ± 0.03	−1.58 ± 0.11	16.45 ± 0.26 (2SD, nAE121 = 14)	16.15 ± 0.26 (2SD, nAE121 = 14)	16.30 ± 0.18	16.7 ± 0.4	95 ± 7	3.61 ± 0.01	69 ± 7	0.38 ± 0.01
FC-12b	*G. menardii*	300–400	1.05 ± 0.03	−0.97 ± 0.11	16.2 ± 0.26 (2SD, nAE121 = 14)		16.20 ± 0.26	14.8 ± 0.4	75 ± 7	3.44 ± 0.01	52 ± 7	0.17 ± 0.01
FC-12b	*N. dutertrei*	300–400	1.35 ± 0.03	−1.57 ± 0.11	17.77 ± 0.24 (2SD, nAE121 = 10)	17.73 ± 0.24 (2SD, nAE121 = 10)	17.75 ± 0.17	17.1 ± 0.4	75 ± 7	3.25 ± 0.01	46 ± 7	0.25 ± 0.01
FC-13a	*G. ruber* (white ss)	250–300	0.08 ± 0.03	−3.71 ± 0.11	20.27 ± 0.24 (2SD, nAE121 = 10)	20.15 ± 0.24 (2SD, nAE121 = 10)	20.21 ± 0.17	16.4 ± 0.4	147 ± 7	4.52 ± 0.01	13 ± 7	0.08 ± 0.01
FC-13a	*T. sacculifer* (without sacc)	300–400	1.59 ± 0.03	−2.46 ± 0.11	17.85 ± 0.29 (2SD, nAE121 = 12)		17.85 ± 0.29	15.7 ± 0.4	121 ± 7	5.49 ± 0.01	21 ± 7	0.49 ± 0.01
FC-13a	*P. obliquiloculata*	300–400	0.00 ± 0.03	−0.97 ± 0.11	16.51 ± 0.26 (2SD, nAE121 = 14)	16.50 ± 0.26 (2SD, nAE121 = 14)	16.51 ± 0.18	18.7 ± 0.4	79 ± 7	4.43 ± 0.01	30 ± 7	0.43 ± 0.01
FC-13a	*G. menardii*	300–400	0.75 ± 0.03	−1.07 ± 0.11	16.74 ± 0.20 (2SD, nAE121 = 6)		16.74 ± 0.20	9.2 ± 0.4	60 ± 7	1.99 ± 0.01	19 ± 7	0.07 ± 0.01
FC-13a	*N. dutertrei*	300–400	0.71 ± 0.03	−1.41 ± 0.11	14.43 ± 0.24 (2SD, nAE121 = 10)	14.40 ± 0.24 (2SD, nAE121 = 10)	14.41 ± 0.17	15.7 ± 0.4	69 ± 7	1.98 ± 0.01	15 ± 7	0.06 ± 0.01
Pacific Ocean												
WP07-a	*G. ruber* (white ss)	250–400			19.12 ± 0.29 (2SD, nAE121 = 12)		19.12 ± 0.29	14.5 ± 0.4	144 ± 7	4.32 ± 0.01	15 ± 7	0.16 ± 0.01
WP07-a	*T. sacculifer* (sacc)	250–400			20.13 ± 0.21 (2SD, nAE121 = 11)		20.13 ± 0.21	12.7 ± 0.4	92 ± 7	4.44 ± 0.01	22 ± 7	0.05 ± 0.01
WP07-a	*T. sacculifer* (without sacc)	250–400			18.10 ± 0.31 (2SD, nAE121 = 11)	18.04 ± 0.31 (2SD, nAE121 = 11)	18.07 ± 0.22	12.3 ± 0.4	192 ± 7	4.51 ± 0.01	21 ± 7	0.08 ± 0.01
WP07-a	*O.universa*	500–630			18.13 ± 0.26 (2SD, nAE121 = 14)	17.99 ± 0.26 (2SD, nAE121 = 14)	18.06 ± 0.18	11.9 ± 0.4	71 ± 7	7.52 ± 0.01	11 ± 7	0.02 ± 0.01
WP07-a	*P. obliquiloculata*	250–400			16.08 ± 0.26 (2SD, nAE121 = 14)	16.19 ± 0.26 (2SD, nAE121 = 14)	16.14 ± 0.18	13.4 ± 0.4	72 ± 7	3.02 ± 0.01	7 ± 7	0.03 ± 0.01
WP07-a	*G. menardii*	250–400			14.74 ± 0.26 (2SD, nAE121 = 14)	14.53 ± 0.26 (2SD, nAE121 = 14)	14.64 ± 0.18	13.5 ± 0.4	85 ± 7	2.68 ± 0.01	26 ± 7	0.08 ± 0.01
WP07-a	*N. dutertrei*	250–400			16.91 ± 0.31 (2SD, nAE121 = 11)	16.99 ± 0.31 (2SD, nAE121 = 11)	16.95 ± 0.22	21.7 ± 0.4	86 ± 7	3.66 ± 0.01	42 ± 7	0.63 ± 0.01
WP07-a	*G. tumida*	250–400			16.45 ± 0.26 (2SD, nAE121 = 14)	16.32 ± 0.26 (2SD, nAE121 = 14)	16.39 ± 0.18	10.6 ± 0.4	58 ± 7	2.55 ± 0.01	16 ± 7	0.10 ± 0.01
806A	*T. sacculifer* (without sacc)	250–400			17.53 ± 0.36 (2SD, nAE121 = 11)		17.53 ± 0.36	14.40 ± 0.4	77 ± 7	3.89 ± 0.01	7 ± 7	0.15 ± 0.01
807A	*T. sacculifer* (without sacc)	250–400			18.38 ± 0.21 (2SD, nAE121 = 11)	18.17 ± 0.21 (2SD, nAE121 = 11)	18.28 ± 0.15	12.54 ± 0.4	87 ± 7	4.24 ± 0.01	17 ± 7	0.09 ± 0.01
A14	*G. ruber* (white ss)	250–400			18.91 ± 0.24 (2SD, nAE121 = 10)	19.17 ± 0.24 (2SD, nAE121 = 10)	19.04 ± 0.17					
A14	*T. sacculifer* (sacc)	250–400			19.53 ± 0.24 (2SD, nAE121 = 10)	19.32 ± 0.24 (2SD, nAE121 = 10)	19.42 ± 0.17	12.0 ± 0.4	102 ± 7	3.91 ± 0.01	22 ± 7	0.02 ± 0.01
A14	*T. sacculifer* (without sacc)	250–400			18.93 ± 0.24 (2SD, nAE121 = 10)	18.84 ± 0.24 (2SD, nAE121 = 10)	18.88 ± 0.17	12.3 ± 0.4	93 ± 7	3.76 ± 0.01	25 ± 7	0.06 ± 0.01
A14	*O. universa*	500–560			17.33 ± 0.26 (2SD, nAE121 = 14)	17.08 ± 0.26 (2SD, nAE121 = 14)	17.20 ± 0.18	11.3 ± 0.4	66 ± 7	6.59 ± 0.01	10 ± 7	0.02 ± 0.01
A14	*N. dutertrei*	250–400			14.39 ± 0.31 (2SD, nAE121 = 11)		14.39 ± 0.31	16.9 ± 0.4	75 ± 7	1.99 ± 0.01	35 ± 7	0.04 ± 0.01

[a] Uncertainties given in 1SD (see text). [b] When two measurements were carried out uncertainty was calculated with $\Delta a = \sqrt{(1/\sum_i (1/\Delta_{ai})^2)}$; with only one measurement the error was determined on reproducibility of the AE121 standard. [c] Uncertainty given in 2SD, calculated on the reproducibility of Cam-Wuellestorfi (see text and Table S3, reference in Misra et al., 2014a).

Table 3. Species-specific $\delta^{11}B_{carbonate}$-to-$\delta^{11}B_{borate}$ calibrations from literature and from our data.

Species	Size fraction (µm)	Material	Instrument (original)	Regression method	$\delta^{11}B_{borate} = f(\delta^{11}B_{calcite})$	n	Calibration number	Reference
G. ruber	∼ 380	Culture/core tops/plankton tows	MC-ICP-MS		$\delta^{11}B_{borate} = [\delta^{11}B_{calcite} - 9.52(\pm2.02)]/0.6(\pm0.11)$			Henehan et al. (2013)
G. ruber	315–355	Core tops	MC-ICP-MS		$\delta^{11}B_{borate} = [\delta^{11}B_{calcite} - 11.78(\pm3.20)]/0.45(\pm0.16)$			Raitzsch et al. (2018)
T. sacculifer	n.d.	Culture/artificial seawater enriched in B	N-TIMS		$\delta^{11}B_{borate} = [\delta^{11}B_{calcite} - 3.94(\pm4.02)]/0.82(\pm0.22)$			Sanyal et al. (2001) refitted Martínez-Boti et al. (2015)
T. sacculifer	315–355	Core tops	MC-ICP-MS		$\delta^{11}B_{borate} = [\delta^{11}B_{calcite} - 8.86(\pm5.27)]/0.59(\pm0.21)$			Raitzsch et al. (2018)
O. universa	no effect	Core tops/plankton tows/sediment traps	MC-ICP-MS		$\delta^{11}B_{borate} = [\delta^{11}B_{calcite} + 0.42(\pm2.85)]/0.95(\pm0.17)$			Henehan et al. (2016)
O. universa	>425	Core tops	MC-ICP-MS		$\delta^{11}B_{borate} = [\delta^{11}B_{calcite} + 5.69(\pm7.51)]/1.26(\pm0.39)$			Raitzsch et al. (2018)
G. bulloides	300–355	Core top/sediment trap	MC-ICP-MS		$\delta^{11}B_{borate} = [\delta^{11}B_{calcite} + 3.440(\pm4.584)]/1.074(\pm0.252)$			Martínez-Boti et al. (2015)
G. bulloides	315–355	Core tops	MC-ICP-MS		$\delta^{11}B_{borate} = [\delta^{11}B_{calcite} + 3.81(\pm13.17)]/1.13(\pm0.72)$			Raitzsch et al. (2018)
N. pachyderma	150-200	Core tops	MC-ICP-MS		$\delta^{11}B_{borate} = \delta^{11}B_{calcite} + 3.38$			Yu et al. (2013)
G. ruber	250–400	Core tops	MC-ICP-MS	Bootstrap	$\delta^{11}B_{borate} = [\delta^{11}B_{calcite} - 9.11(\pm0.73)]/0.58(\pm0.91)$	9	0	This study, Henehan et al. (2013)
G. ruber	250–400	Core tops	MC-ICP-MS	Bootstrap	$\delta^{11}B_{borate} = [\delta^{11}B_{calcite} + 1.23(\pm0.59)]/1.12(\pm1.67)$	5	1	This study
G. ruber	250–455	Core tops	MC-ICP-MS	Bootstrap	$\delta^{11}B_{borate} = [\delta^{11}B_{calcite} - 11.73(\pm0.83)]/0.46(\pm0.34)$	40	2	This study; Foster et al. (2008), Henehan et al. (2016), Raitzsch et al. (2018)
T. sacculifer (sacc and without sacc)	250–400	Core tops	MC-ICP-MS	Bootstrap	$\delta^{11}B_{borate} = [\delta^{11}B_{calcite} + 6.06(\pm0.25)]/1.38(\pm1.33)$	11	3	This study
T. sacculifer (sacc and without sacc)	250–400	Core tops	MC-ICP-MS	Bootstrap	$\delta^{11}B_{borate} = [\delta^{11}B_{calcite} - 4.09(\pm0.86)]/0.83(\pm0.48)$	27	4	This study; Foster et al. (2008), Raitzsch et al. (2018)
N. dutertrei	300–400	Core tops	MC-ICP-MS	Bootstrap	$\delta^{11}B_{borate} = [\delta^{11}B_{calcite} - 0.34(\pm1.83)]/0.93(\pm0.55)$	5	5	This study
N. dutertrei	300–400	Core tops	MC-ICP-MS	Bootstrap	$\delta^{11}B_{borate} = [\delta^{11}B_{calcite} - 3.88(\pm0.65)]/0.72(\pm0.74)$	9	6	This study; Foster et al. (2008)
O. universa	400–600	Core tops	MC-ICP-MS	Bootstrap	$\delta^{11}B_{borate} = [\delta^{11}B_{calcite} + 8.01(\pm23)]/1.38(\pm2.67)$	5	7	This study
O. universa	400–600	Core tops	MC-ICP-MS	Bootstrap	$\delta^{11}B_{borate} = [\delta^{11}B_{calcite} + 2.08(\pm0.59)]/1.06(\pm0.13)$	36	8	This study; Henehan et al. (2016), Raitzsch et al. (2018)
G. menardii	400–600	Core tops	MC-ICP-MS	Bootstrap	$\delta^{11}B_{borate} = [\delta^{11}B_{calcite} - 5.36(\pm1.36)]/0.65(\pm0.76)$	5	9	This study
G. tumida	400–600	Core tops	MC-ICP-MS	Bootstrap	$\delta^{11}B_{borate} = [\delta^{11}B_{calcite} - 6.33(\pm2.52)]/0.57(\pm1.2)$	3	10	This study
P. obliquiloculata	300–400	Core tops	MC-ICP-MS	Bootstrap	$\delta^{11}B_{borate} = [\delta^{11}B_{calcite} - 5.59(\pm4.16)]/0.59(\pm0.65)$	6	11	This study; Henehan et al. (2016)
Deep-dweller	300–600	Core tops	MC-ICP-MS	Bootstrap	$\delta^{11}B_{borate} = [\delta^{11}B_{calcite} - 1.99(\pm0.13)]/0.82(\pm0.27)$	22	12	This study
Deep-dweller	300–600	Core tops	MC-ICP-MS	Bootstrap	$\delta^{11}B_{borate} = [\delta^{11}B_{calcite} - 0.18(\pm0.6)]/0.95(\pm0.13)$	54	13	This study; Foster et al. (2008), Henehan et al. (2016), Raitzsch et al. (2018)

n.d.: not determined.

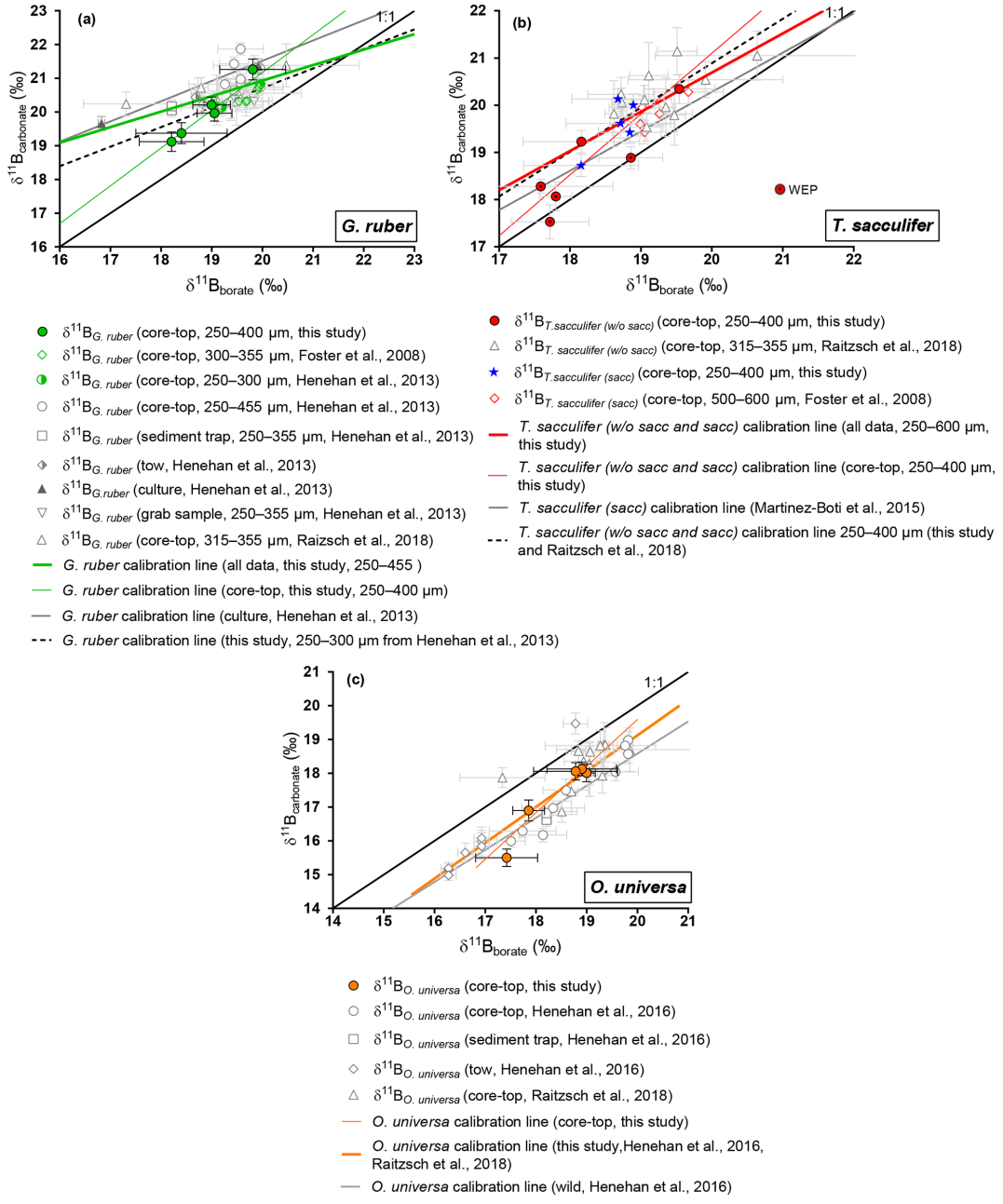

Figure 4. Boron isotopic measurements of mixed-layer foraminifera plotted against $\delta^{11}B_{borate}$. $\delta^{11}B_{borate}$ was characterized by determination of the calcification depth of foraminifera utilizing data presented in Fig. 3. **(a)** *G. ruber*, **(b)** *T. sacculifer*, **(c)** *O. universa*. Monospecific calibrations (Table 3) and error bars on $\delta^{11}B_{borate}$ were derived utilizing the wild bootstrap code from Henehan et al. (2016), while errors on the $\delta^{11}B_{carbonate}$ for this study are reported as 2σ of measured AE121 standards during the session of the sample. Calibrations were also derived on the 250–400 size fraction for *G. ruber* and *T. sacculifer* (black dashed lines). Data reported on those graphs have been measured with an MC-ICP-MS.

alone yields a slope of 1.3 ± 0.2 but is not statistically different to the results from Martínez-Boti et al. (2015b) (Table 3), ($p > 0.05$). However, when compiled with published data using the bootstrap method a slope of 0.83 ± 0.48 is calculated, with a large uncertainty given the variability in the data. It is also noticeable that *T. sacculifer* (without sacc) samples from the WEP have a $\delta^{11}B_{carbonate}$ close to expected $\delta^{11}B_{borate}$ and are significantly lower compared to the combined *T. sacculifer* of other sites ($p = 0.01$, unpaired t test). When regressing data from the 250–400 µm fraction, our results are not significantly different from the regression through data that combine all size fractions (Fig. 4).

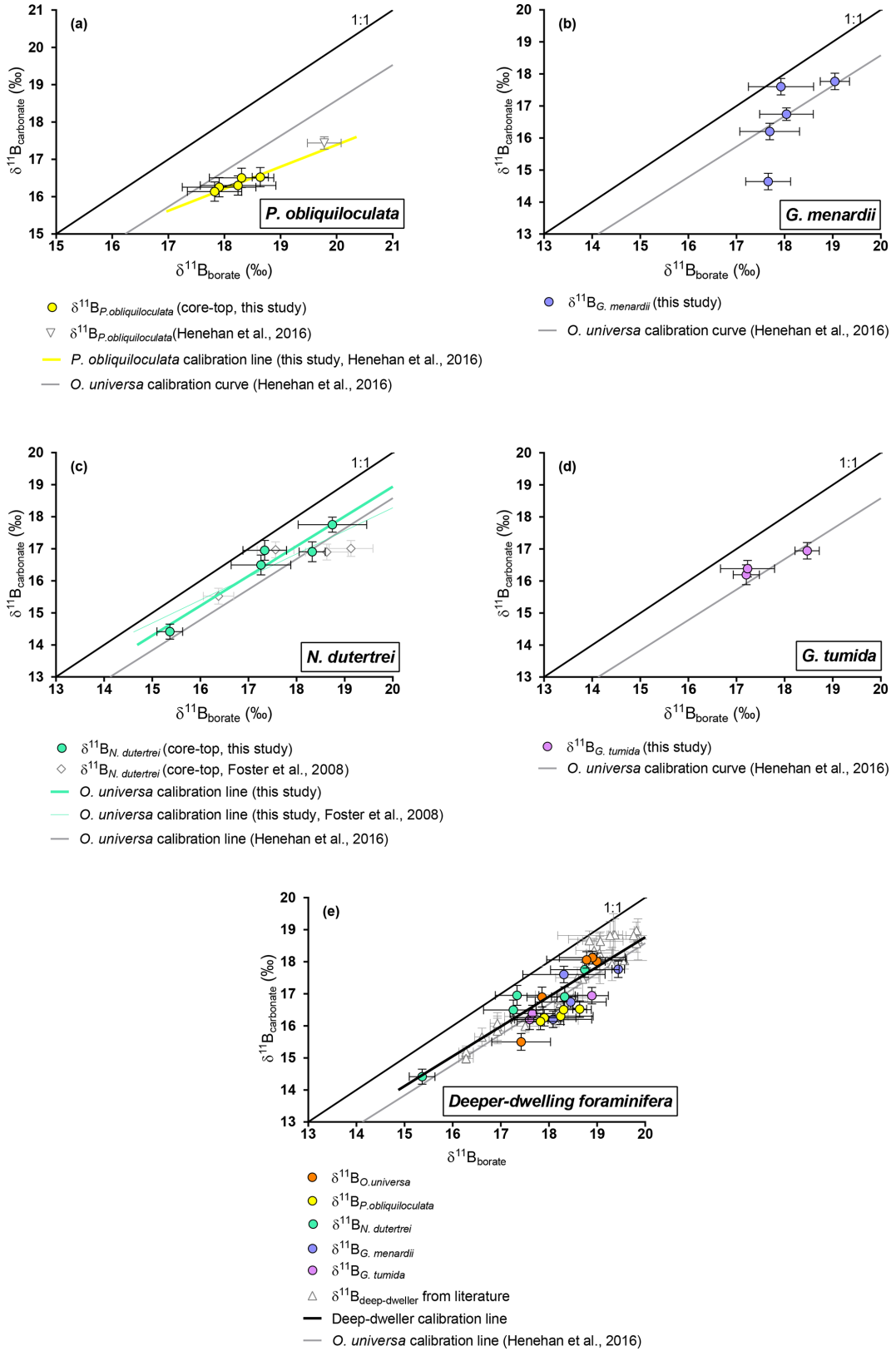

Figure 5. Boron isotopic measurements of deep-dwelling foraminifera ($\delta^{11}B_{carbonate}$) plotted against $\delta^{11}B_{borate}$. $\delta^{11}B_{borate}$ was constrained using foraminiferal calcification depths. **(a)** *P. obliquiloculata*, **(b)** *G. menardii*, **(c)** *N. dutertrei*, **(d)** *G. tumida*. **(e)** Compilation of deep dweller species. Monospecific calibrations are summarized in Table 3.

4.2.3 *O. universa* and deeper-dwelling species: *N. dutertrei, P. obliquiloculata, G. menardii* , and *G. tumida*

Our results for *O. universa* (Fig. 4), *N. dutertrei, P. obliquiloculata, G. menardii*, and *G. tumida* (Fig. 5) exhibit lower $\delta^{11}B_{carbonate}$ compared to the expected $\delta^{11}B_{borate}$ at their collection location. These data for *O. universa* are not statistically different from the Henehan et al. (2016) calibration ($p>0.05$). Our results for *N. dutertrei* expand upon the initial measurements presented in Foster et al. (2008). The different environments experienced by *N. dutertrei* in our study permit us to extend the range and derive a calibration for this species; the slope is close to unity (0.93 ± 0.55) and is not significantly different ($p>0.05$) from the *O. universa* calibration previously reported by Henehan et al. (2016) (e.g., 0.95 ± 0.17). The data for *P. obliquiloculata* exhibit the largest offset from the theoretical line. The range of $\delta^{11}B_{borate}$ from the samples we have of *G. menardii* and *G. tumida* is not sufficient to derive calibrations, but the $\delta^{11}B_{carbonate}$ measured for those species is in good agreement with the *N. dutertrei* calibration and Henehan et al. (2016) calibration for *O. universa*.

For *O. universa* and all deep-dwelling species, the slopes are not statistically different from Henehan et al. (2016) ($p>0.05$) and are close to unity. If data for deep-dwelling foraminiferal species are pooled together with each other and with data from Henehan et al. (2016) and Raitzch et al. (2018), we calculate a slope of 0.95 (± 0.13) ($R^2 = 0.7987$, $p<0.0001$); if only our data are used, we calculate a slope that is not significantly different (0.82 ± 0.27; $p<0.05$).

4.2.4 Comparison of core-top and culture data

The data for *G. ruber* and *T. sacculifer* from the core tops we measured are broadly consistent with previous published results. The calibrations between these core-top-derived estimates and culture experiments are not statistically different due to small datasets and uncertainties on the linear regressions (Henehan et al., 2013; Marinez-Boti et al., 2015; Raitzsch et al., 2018; Table 3). The sensitivities of the species analyzed are not statistically different and are close to unity.

4.3 B/Ca ratios

B/Ca ratios are presented in Table 2 and Fig. 6. B/Ca data are species-specific and consistent with previous work (e.g., compiled in Henehan et al., 2016) with ratios higher for *G. ruber* > *T. sacculifer* (sacc) > *T. sacculifer* (without sacc) > *P. obliquiloculata* > *O. universa* >> *G. menardii* > *N. dutertrei* > *G. tumida* > *G. inflata* > *N. pachyderma* > *G. bulloides* (Fig. 6). This study supports species-specific B/Ca ratios as previously published (Yu et al., 2007; Tripati et al., 2009, 2011; Allen and Hönisch, 2012; Henehan et al., 2016). Differences between surface- and deep-dwelling foraminifera are observed, with lower values and a smaller range for the deeper-dwelling taxa (58–126 µmol mol^{-1} vs. 83–190 µmol mol^{-1} for shallow dwellers); however, the trend for the surface dwellers can also be driven by interspecies B/Ca variability. The B/Ca data for deep-dwelling taxa exhibit a significant correlation with $[B(OH)_4^-]/[HCO_3^-]$ ($p<0.05$) but no correlation with $\delta^{11}B_{carbonate}$, and temperature (Fig. S3). Surface-dwelling species have B/Ca ratios that exhibit significant correlations with $[B(OH)_4^-]/[HCO_3^-]$, $\delta^{11}B_{carbonate}$ and temperature. The sensitivity of B/Ca to $[B(OH)_4^-]/[HCO_3^-]$ is lower for deep-dwelling species compared to surface-dwelling species. When all the B/Ca data are compiled, significant trends are observed with $[B(OH)_4^-]/[HCO_3^-]$, $\delta^{11}B_{carbonate}$, and temperature (Fig. S3). When comparing data from all sites together, a weak decrease in B/Ca with increasing calcification depth is observed ($R^2 = 0.11$, $p<0.05$, Fig. S4). A correlation also exists between B/Ca and the water depths of the cores (not significant, Fig. S4).

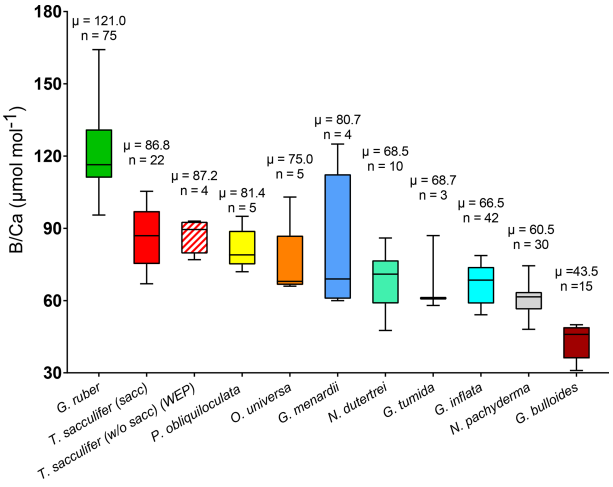

Figure 6. Box plots of B/Ca ratios for multiple foraminifera species., including *T. sacculifer* (this study; Foster et al., 2008; Ni et al; 2007; Seki et al., 2010), *G. ruber* (this study; Babila et al., 2014; Foster et al., 2008; Ni et al., 2007), *G. inflata*, *G. bulloides* (Yu et al., 2007), *N. pachyderma* (Hendry et al., 2009; Yu et al., 2013), *N. dutertrei* (this study; Foster et al., 2008), *O. universa*, *P.obliquiloculata, G. menardii*, and *G. tumida* (this study).

5 Discussion

5.1 Sources of uncertainty relating to depth habitat and seasonality at studied sites

5.1.1 Depth habitats and $\delta^{11}B_{borate}$

Because foraminifera will record ambient environmental conditions during calcification, the accurate characterization of in situ data is needed not only for calibrations but also

to understand the reconstructed record of pH or pCO_2. The species we examined are ordered here from shallower to deeper depth habitats: *G. ruber* > *T. sacculifer* (sacc) > *T. sacculifer* (without sacc) > *O. universa* > *P. obliquiloculata* > *G. menardii* > *N. dutertrei* > *G. tumida* (this study; Birch et al., 2013; Farmer et al., 2007), although the specific water depth will vary depending on the physical properties of the water column of the site (Kemle-von Mücke and Oberhänsli, 1999). We note that calculation of absolute calcification depths can be challenging in some cases as many species often transition to deeper waters at the end of their life cycle prior to gametogenesis (Steinhardt et al., 2015).

We find that assumptions about the specific depth habitat a species of foraminifera is calcifying over, in a given region, can lead to differences of a few per mill in calculated isotopic compositions of borate (Fig. 3). Hence this can cause a bias in calibrations if calcification depths are assumed instead of being calculated (i.e., with $\delta^{18}O$ and/or Mg/Ca). Factors including variations in thermocline depth can impact depth habitats for some taxa. At the sites we examined, most of the sampled species live in deeper depth habitats in the WEP relative to the Indian Ocean, which in turn is characterized by deeper depth habitats than in the Arabian Sea. In the tropical Pacific, *T. sacculifer* is usually found deeper than *G. ruber* except at sites characterized by a shallow thermocline, in which case both species tend to overlap their habitat (e.g., ODP Site 806 in the WEP which has a deeper thermocline than at ODP Site 847 in the eastern equatorial Pacific, EEP) (Rickaby et al., 2005). The difference in depth habitats for *T. sacculifer* and *N. dutertrei* between the WEP and EEP can be as much as almost 100 m (Rickaby et al., 2005).

5.1.2 Seasonality and in situ $\delta^{11}B_{borate}$

As discussed by Raitzsch et al. (2018), depending on the study area, foraminiferal fluxes can change throughout the year. Hydrographic parameters related to carbonate chemistry may change across seasons at a given water depth. We therefore recalculated the theoretical $\delta^{11}B_{borate}$ using seasonal data for temperature and salinity and annual values for TA and DIC for each depth at each site. The GLODAP (2013) (Key et al., 2004) database does not provide seasonal TA or DIC values.

The low sensitivity of $\delta^{11}B_{borate}$ to temperature and salinity means that calculated $\delta^{11}B_{borate}$ values for each water depth at our sites were not strongly impacted (Fig. S1 in the Supplement). Thus, these findings support Raitzsch et al. (2018), who concluded that calculated $\delta^{11}B_{borate}$ values corrected for seasonality were within the error of non-corrected values for each water depth. As Raitzsch et al. (2018) highlight, seasonality might be more important at high-latitude sites where seasonality is more marked; however, the seasonality of primary production will also be more tightly constrained due to the seasonal progression of winter light limitation and intense vertical mixing and summer nutrient limitation.

Data for our sites suggest that most $\delta^{11}B_{borate}$ variability we observe does not come from seasonality but from the assumed water depths for calcification. With the exception of a few specific areas such as the Red Sea (Henehan et al., 2016; Raitzsch et al., 2018), at most sites examined seasonal $\delta^{11}B_{borate}$ at a fixed depth does not vary by more than ~ 0.2 ‰. We conclude that seasonality has a relatively minor impact on the carbonate system parameters at the sites we examined.

5.2 $\delta^{11}B$, microenvironment pH, and depth habitats

It is common for planktonic foraminifera to have symbiotic relationships with algae (Gast and Caron, 2001; Shaked and de Vargas, 2006). The family Globigerinidae, including *G. ruber*, *T. sacculifer*, and *O. universa*, commonly has dinoflagellate algal symbionts (Anderson and Be, 1976; Spero, 1987). The families Pulleniatinidae and Globorotaliidae (e.g., *P. obliquiloculata, G. menardii*, and *G. tumida*) have chrysophyte algal symbionts (Gastrich, 1988) and *N. dutertrei* hosts pelagophyte symbionts (Bird et al., 2018). The relationship between the symbionts and the host is complex. Nevertheless, this symbiotic relationship provides energy (Hallock, 1981b) and promotes calcification in foraminifera (Duguay, 1983; Erez et al., 1983) by providing inorganic carbon to the host (Jørgensen et al., 1985).

There are several studies indicating that the $\delta^{11}B$ signatures in foraminiferal calcite reflect microenvironment pH (Jørgensen et al., 1985; Rink et al., 1998; Köhler-Rink and Kühl, 2000; Hönisch et al., 2003; Zeebe et el., 2003). Foraminifera with high photosynthetic activity and symbiont density, such as *G. ruber* and *T. sacculifer*, are expected to have a microenvironment pH higher than ambient seawater and a $\delta^{11}B_{carbonate}$ higher than expected $\delta^{11}B_{borate}$, which is the case in our study and in previous studies (Foster et al., 2008; Henehan et al., 2013; Raitzsch et al., 2018). We also observed in our study that *N. dutertrei*, *G. menardii*, *P. obliquiloculata*, and *G. tumida* record a lower pH than ambient seawater, with $\delta^{11}B_{carbonate}$ lower than expected $\delta^{11}B_{borate}$, and we suggest the results are consistent with lower photosynthetic activity compared to the mixed-layer dwelling species. These observations, based on $\delta^{11}B_{carbonate}$ measurements, are in line with direct observations from Takagi et al. (2019) that show dinoflagellate-bearing foraminifera (*G. ruber*, *T. sacculifer*, and *O. universa*) tend to have a higher symbiont density and photosynthesis activity while *P. obliquiloculata*, *G. menardii*, and *N. dutertrei* have lower symbiont density and *P. obliquiloculata* and *N. dutertrei* have the lowest photosynthetic activity. In the same study, *P. obliquiloculata* exhibited minimum symbiont densities and levels of photosynthetic activity, which may explain why *P. obliquiloculata* exhibited the lowest microenvironment pH as recorded by $\delta^{11}B$.

Based on the observations of Takagi et al. (2019), we can assume that the low $\delta^{11}B$ of *O. universa* and *T. sacculifer* (without sacc) from the WEP is explained by low photosynthetic activity. It has been shown for *T. sacculifer* and *O. universa* that symbiont photosynthesis increases with higher insolation (Jørgensen et al., 1985; Rink et al., 1998) and the photosynthetic activity is therefore a function of the light level the symbionts received. This is, in a natural system, dependent on the depth of the species in the water column. For the purpose of this study, we do not consider turbidity which also influences the light penetration in the water column. In this case, photosynthetically active foraminifera living close to the surface should record microenvironment pH (thus $\delta^{11}B$) that is more sensitive to water depth changes. A deeper habitat reduces solar insolation, and as a consequence may lower symbiont photosynthetic activity, possibly reducing pH in the foraminifera's microenvironment. This is supported by the significant trend observed between $\Delta^{11}B$ and the calcification depth for *G. ruber* and *T. sacculifer* at our sites (Fig. S2), where microenvironment pH decreases with calcification depth. We observe a significant decrease in $\delta^{11}B$ in the WEP for *T. sacculifer* (without sacc) compared to the other sites ($p<0.05$). Additionally, the $\Delta^{11}B$ ($\Delta^{11}B=\delta^{11}B_{carbonate}-\delta^{11}B_{borate}$) of *G. ruber* and *T. sacculifer* (without sacc and sacc) is significantly lower in the WEP compared to the other sites ($p<0.05$).

T. sacculifer has the potential to support more photosynthesis due to its higher symbiont density, and higher photosynthetic activity compared to other species, which may support higher symbiont–host interactions (Takagi et al., 2019). These results would be consistent with a greater sensitivity of *T. sacculifer*'s photosynthetic activity with changes in insolation–water depth. To test if the low $\delta^{11}B$ signature of *T. sacculifer* (without sacc) in the WEP is related to a decrease in light at greater water depth, we have independently calculated the calcification depth of the foraminifera based on various light insolation culture experiments (Jørgensen et al., 1985) and the microenvironment ΔpH derived from our data (Fig. 7a and b). This exercise showed that the low $\delta^{11}B$ of *T. sacculifer* (without sacc) from the WEP can be explained by the reduced light environment due to a deeper depth habitat in the WEP (Fig. 7b). It can also be noted that *T. sacculifer* exhibits the largest variation in symbiont density versus test size (Takagi et al., 2019), suggesting that lower size fraction reported for the WEP (250–400 µm) compared to the 300–400 µm at the other sites can be related to a decrease in photosynthetic activity and a lower $\delta^{11}B$. Unfortunately, no weight-per-shell data were determined on foraminifera samples to constrain whether test size was significantly different across sites. Future studies could use shell weights to test these relationships.

When the same approach of independently reconstructing calcification depth based on culture experiments is applied to *O. universa*, the boron data suggest a microenvironment pH of 0.10 to 0.20 lower than ambient seawater pH, which would be in line with the species living deeper than 50 m (light compensation point (Ec); Rink et al., 1998), which is consistent with our calcification depth reconstructions. The low $\delta^{11}B_{carbonate}$ of *O. universa* compared to *T. sacculifer* for the similar calcification depth at some sites (e.g., FC-02a, WP07-a) might reflect differences in photosynthetic potential between the two species, which is supported by observation of a lower photosynthetic potential in *O. universa* than in *T. sacculifer* (Tagaki et al., 2019).

Microenvironment ΔpH based on our $\delta^{11}B_{carbonate}$ data was calculated for the rest of the species. We observed that microenvironment ΔpH is higher in *T. sacculifer* > *G. ruber* > *T. sacculifer* (without sacc – WEP) > *O. universa*, *N. dutertrei*, *G. menardii*, *G. tumida* > *P. obliquiloculata*. These results are in line with the photosymbiosis findings from Takagi et al. (2019). Also, the higher $\delta^{11}B$ data from the west African upwelling published by Raitzsch et al. (2018) for *G. ruber* and *O. universa* may reflect a higher microenvironment pH due to a relatively shallow habitat, higher insolation, and high rates of photosynthesis by symbionts. This could highlight a potential issue with calibration when applied to sites with different oceanic regimes as the $\delta^{11}B$ species-specific calibrations could also be location-specific for the mixed dweller species.

Microenvironment pH for *N. dutertrei, G. menardii*, and *G. tumida* is similar to *O. universa* and suggests a threshold for a respiration-driven $\delta^{11}B$ signature. This threshold can be induced by a change of photosynthetic activity at lower light intensity in deeper water and/or differences in symbiont density and/or by the type of symbionts at greater depth (non-dinoflagellate symbionts). We also note that *P. obliquiloculata,* which has the lowest symbiont density and photosynthetic activity (Takagi et al., 2019), has the lowest microenvironment pH compared to other deeper-dweller species, supporting our hypothesis that respiration can control microenvironment pH. The deep-dwelling species sensitivity of $\delta^{11}B_{carbonate}$ to $\delta^{11}B_{borate}$ with values close to unity might also be explained by relatively stable respiration-driven microenvironments, as the deeper-dweller species do not experience large changes of insolation (e.g., photosynthesis), thereby making them a more direct recorder of environmental pH.

5.3 $\delta^{11}B$ sensitivity to $\delta^{11}B_{borate}$ and relationship with B/Ca signatures

In inorganic calcite, $\delta^{11}B_{carbonate}$ and B/Ca data have shown to be sensitive to precipitation rate with a higher precipitation rate increasing $\delta^{11}B_{carbonate}$ (Farmer et al., 2019) and B/Ca (Farmer et al., 2019; Gabitov et al., 2014; Kaczmarek et al., 2016; Mavromatis et al., 2015; Uchikawa et al., 2015). A recent study from Farmer et al. (2019) has proposed that in foraminifera at higher precipitation rates, more borate ions may be incorporated into the carbonate mineral, while more boric acid may be incorporated at lower precipitation rates.

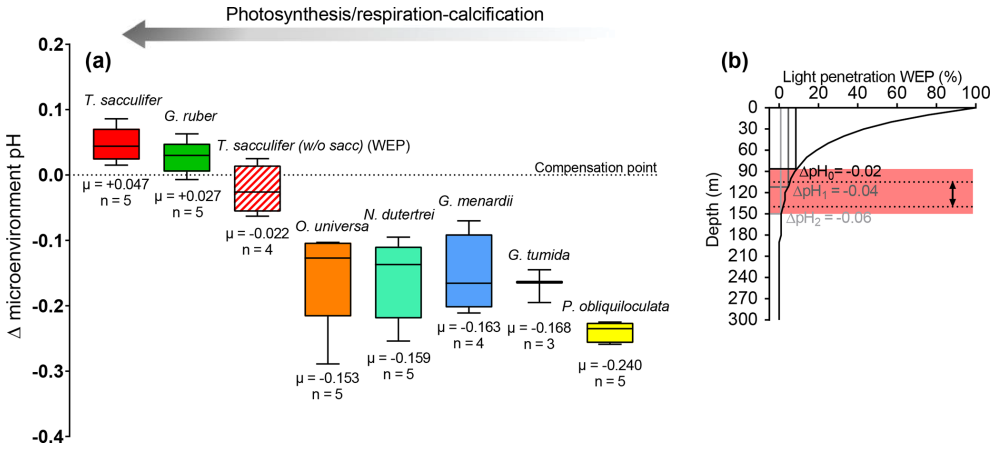

Figure 7. (a) Box plot showing the calculated microenvironment pH difference (Δ microenvironment pH) between microenvironment and external pH based on the δ^{11}B data. **(b)** This figure shows that a decrease in insolation can explain the low δ^{11}B from the WEP. Light penetration profile in the western Pacific, with E_0 in the WEP of 220 J s^{-1} m^{-2} (Weare et al., 1981) and a light attenuation coefficient of 0.028 (m^{-1}) (Wang et al., 2008). Theoretical depths were calculated for a decrease in microenvironment pH of $\Delta pH_1 = -0.02$ (e.g., WP07-a); $\Delta pH_1 = -0.04$ (e.g., A14), $\Delta pH_2 = -0.06$ (e.g., 806A). Light penetration corresponding to Ec is ∼ 12 %, $\Delta pH_0 \sim 7$ %, $\Delta pH_1 \sim 5$ %, $\Delta pH_2 \sim 1$ %, and respective calcification depths are 75, 90, 110, and 150 m. The grey band is the calcification depth calculated that explains the Δ microenvironment pH from ΔpH_0 to ΔpH_2. Dotted lines show the range of the calcification depth for *T. sacculifer* (without sacc) in the WEP utilized in this study.

The authors also suggest this may explain low sensitivities of culture experiments.

When combining all literature data, *T. sacculifer* and *G. ruber* have sensitivities of $\delta^{11}B_{carbonate}$ to $\delta^{11}B_{borate}$ of 0.83± 0.48 and 0.46±0.34, respectively, in line with previous literature and paleo-CO_2 reconstructions. Also, if we only take into account our data, and the observation that the sensitivity of $\delta^{11}B_{carbonate}$ to $\delta^{11}B_{borate}$ is not statistically different from unity for most of the species investigated, we can speculate that for these taxa, changes in precipitation rate and contributions of boric acid are not likely to be important. If considering only the data from this study, *G. ruber* (1.12 ± 1.67) and *T. sacculifer* (1.38 ± 1.35) present higher sensitivities of $\delta^{11}B_{carbonate}$ to $\delta^{11}B_{borate}$. We can then again speculate that the observed high values for $\delta^{11}B_{carbonate}$ at high seawater pH can be due to higher precipitation rates. We note this could also be consistent with the higher sensitivity of B/Ca signatures in these two surface dwelling species to ambient $[B(OH)_4^-]/[HCO_3^-]$ relative to deeper-dwelling species. Those interspecific differences still remain to be explained; however, part of this variability is likely due to changes in the carbonate chemistry of the microenvironment resulting in changing competition between borate and bicarbonate. A caveat is that we can not exclude specific biological processes and that in taxa with a non-respiration-driven microenvironment, changes in day / night calcification ratios also impact observed values. As indicated by Farmer et al. (2019), studies of calcite precipitation rates in foraminifera may help to improve our understanding of the fundamental basis of boron-based proxies.

5.4 Evaluation of species for pH reconstructions and water depth pH reconstructions

This data set allows us to reassess the utility of boron-based proxies for the carbonate system. The main aim of using boron-based proxies relates to the reconstruction of past oceanic conditions, specifically pH and pCO_2. Mixed-layer species (e.g., *G. ruber* and *T. sacculifer)* are potential archives for atmospheric CO_2 reconstructions. Other species can shed light on other aspects of the carbon cycle including the physical and biological carbon pumps.

There are a few main inferences we can make. When integrated with published data, the sensitivities of $\delta^{11}B_{carbonate}$ to $\delta^{11}B_{borate}$ for *G. ruber* and *T. sacculifer* are similar to those in previous studies (Martínez-Boti et al., 2015b; Raitzsch et al., 2018), which supports the fidelity of previous paleo-reconstructions that use published calibrations between $\delta^{11}B_{carbonate}$ and $\delta^{11}B_{borate}$. The regression we have made for *G. ruber* supports a decrease in $\delta^{11}B_{carbonate}$ with decreasing size fractions (offset of −0.4 ‰, $p>0.05$) with the sensitivity of $\delta^{11}B_{carbonate}$ to $\delta^{11}B_{borate}$ not being statistically different from a higher size fraction ($p<0.05$). The variability in our weight per shell for our *G. ruber*, based on data from Henehan et al. (2013), can potentially imply a deviation down to 1 ‰ relative to the calibration line from Henehan et al. (2013), which can be in line with the maximum deviation observed in our data (∼ 1.2 ‰) and not inconsistent with a size effect explaining the offset in our calibration. Our $\delta^{11}B_{carbonate}$ data and the sensitivity to $\delta^{11}B_{borate}$ of *O. universa* support previous data from Henehan et al. (2016). *N. dutertrei* $\delta^{11}B_{carbonate}$ data span a large range of pH, al-

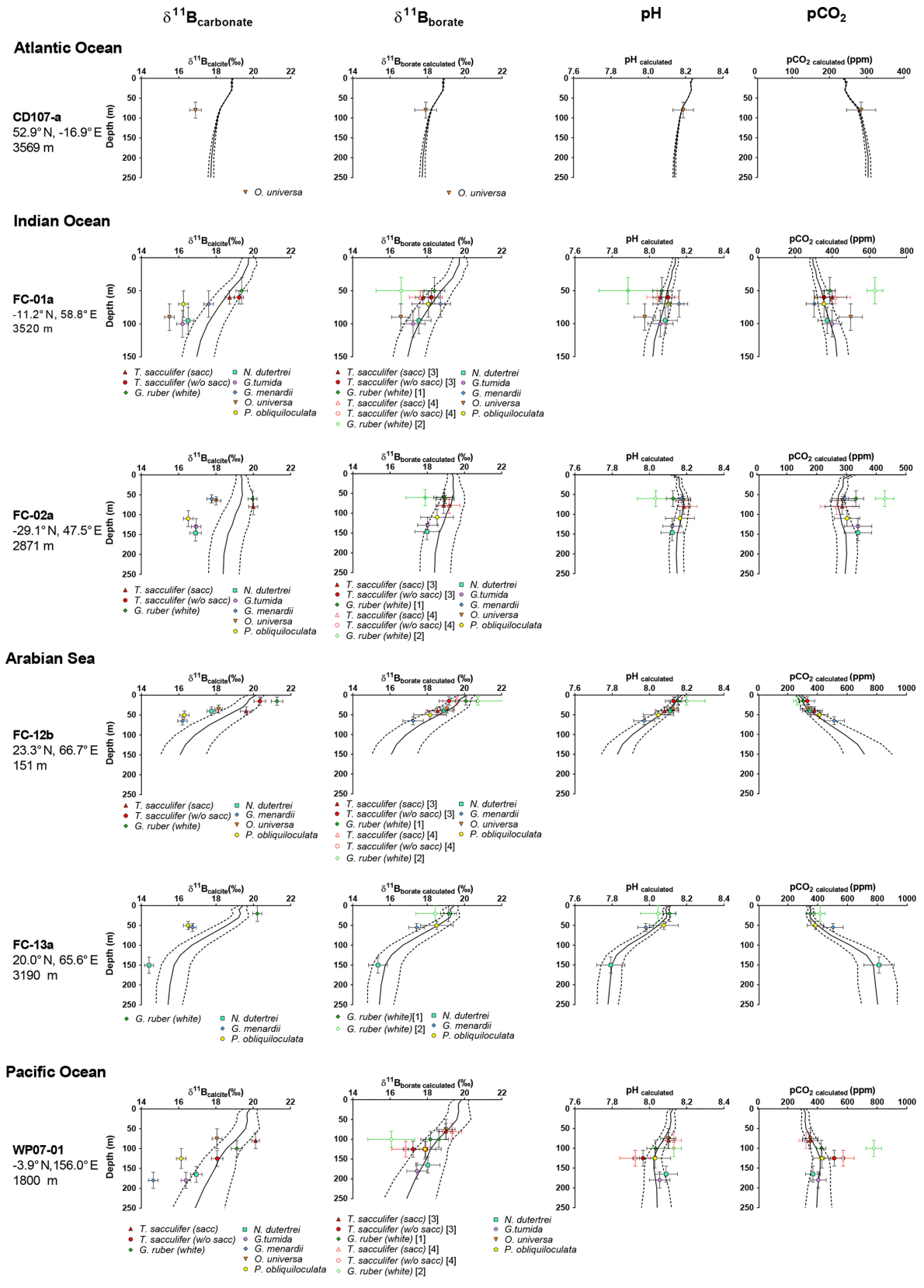

Figure 8. Water depth pH profiles reconstructed at every site applying the monospecific calibrations derived from our results (Table 3). The figure shows measured $\delta^{11}B_{calcite}$, $\delta^{11}B_{borate}$ calculated according to different calibrations (see Table 3 and text), calculated pH based on $\delta^{11}B$ ($pH_{\delta^{11}B}$), and pCO_2 calculated from $pH_{\delta^{11}B}$ and alkalinity.

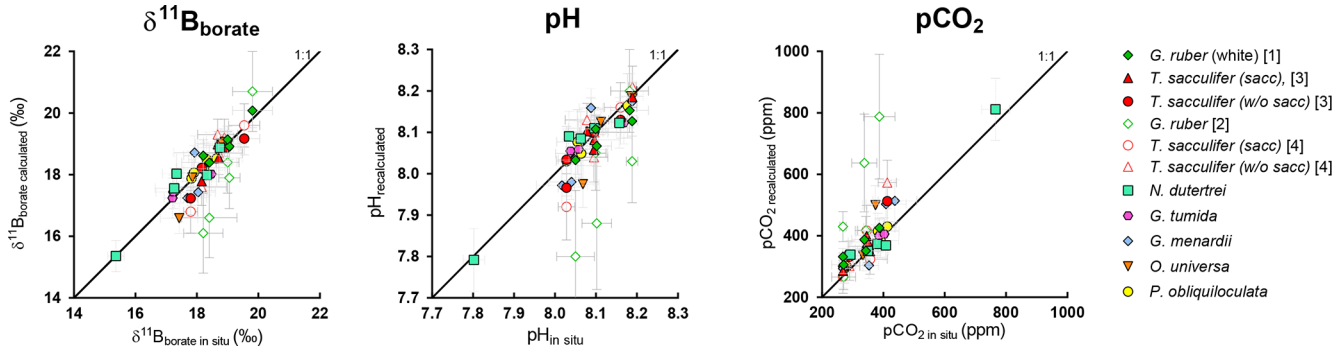

Figure 9. Evaluation of the reconstructed parameters, $\delta^{11}B_{borate}$, pH, and pCO_2 versus in situ parameters calculated in Fig. 8 (based on $\delta^{11}B$ and alkalinity). The recalculated parameters are consistent with in situ data, except for *G. ruber*, and this variability might be explained by the different test sizes within measured size fractions.

lowing us to derive a robust calibration with $\delta^{11}B_{borate}$. It remains premature to assume that a unique calibration with a slope of ~ 0.9 can be used for all deeper-dwelling species. More data are needed for *P. obliquiloculata*, *G. menardii*, and *G. tumida* to robustly test this assertion.

In order to derive accurate reconstructions of past ambient pH and pCO_2, accurate species-specific calibrations need to be used that are constrained by core tops or samples from similar types of settings (Figs. 8, 10, S6). Lower $\delta^{11}B$ signatures in *T. sacculifer* (without sacc) are observed in the WEP, which may be explained by the deeper depth habitat for this taxa, as lower light levels might reduce symbiont photosynthetic activity. Also, we show that a correction is needed for *T. sacculifer* (without sacc) in the WEP in order to accurately reconstruct atmospheric CO_2. When applying calibrations nos. 2 and 4 to *T. sacculifer* and *G. ruber* (compilation of all data, Table 3), our data show more variability, especially for *G. ruber* which leads to the larger mismatch compared to in situ parameters. The greater divergence of reconstructed values from in situ measurements is observed at site WPO7-01 for both *T. sacculifer* (without sacc) and *G. ruber*. More data would be needed to determine a proper correction for both species and a core-top study will be determinant for future downcore reconstructions, especially in the WEP. We also find that for two species the boron isotope proxy is a relatively straightforward recorder of ambient pH, with sensitivities close to unity observed for *O. universa* and *N. dutertrei*.

There is also promise in using multiple species in a sample from different hydrographic regimes to reconstruct vertical profiles of pH and pCO_2. We are able to reproduce pH and pCO_2 profiles from multiple sites with different water column structures (Fig. 8) with those reconstructions within error of the in situ values, for most sites. In order to avoid circularity, to validate these calibrations, we recalculated ambient pH and pCO_2 by first excluding site-specific data and then recalculating species-specific calibrations, followed by application to each specific site. The comparison of the two methods, first using all the data to derive the calibration and recalculate pH and pCO_2 (circular) and second by excluding the site of interest, deriving calibrations, and calculating pH and pCO_2 (not circular), does not show significant differences and validates the robustness of the calibrations (Fig. S5). We utilized the calibrations derived from our data for *G. ruber* (calibration nos. 1 and 2, Table 3), *T. sacculifer* (calibration nos. 3 and 4, Table 3), *O. universa* (calibration no. 8, Table 3), and *P. obliquiloculata* (calibration no. 11, Table 3), and for *N. dutertrei*, *G. tumida*, and *G. menardii* we utilized the calibration on the compilation of the deep dwellers (calibration no. 13, Table 3). Results are shown in Fig. 8 and evaluated in Fig. 9. For *G. menardii*, more data would be helpful to provide additional constraints. Results for *G. ruber* are the most scattered, potentially due to difference in test sizes (Henehan et al., 2013) or depth habitat. Results reaffirm the importance of working with narrow size fractions (Henehan et al., 2013), the utilization of calibrations derived from the same size fraction, or use of offsets to take into account this size fraction effect and the importance of core-top studies before paleo-application.

6 Conclusions and future implications

Our study has extended the boron isotope proxy with data for new species and sites. The work supports previous work showing that depth habitats of foraminifera vary depending on the oceanic regime, and this can impact boron isotope signatures. Low $\delta^{11}B$ values in the WEP compared to other regions for *T. sacculifer* (without sacc) may be explained by a reduction in microenvironment pH due to a deeper depth habitat associated with reduced irradiance and thus photosynthetic activity.

In order to accurately develop downcore reconstructions, constraining the depth habitat using core-top studies is important, as the same species can record the seawater pH at different water depths, potentially introducing biases when comparing between different locations. Also, we speculate

that a change of the thermocline depth in the past could imply variations in depth habitat and introduce biases in the reconstructions, but further work is needed to test this assertion.

The sensitivity of $\delta^{11}B_{carbonate}$ to pH is in line with previously published data for *T. sacculifer* and *G. ruber*. The sensitivity of $\delta^{11}B_{carbonate}$ to pH of *O.universa* (mixed dweller), *N. dutertrei*, *G. menardii*, and *G. tumida* (deep dwellers) is similar, but more data are needed to fully determine those sensitivities. The similarity of boron isotope calibrations for deep-dwelling taxa might be related to similar respiration-driven microenvironments.

Reconstruction of seawater pH and carbonate system parameters is achievable using foraminiferal $\delta^{11}B$, but additional core-top and down-core studies reconstructing depth profiles will be needed in order to further verify calibrations published to date. Past pH and pCO_2 water depth profiles can potentially be created by utilizing multiple foraminiferal species in concert with taxon-specific calibrations for similar settings. This approach has much potential for enhancing our understanding of the past workings of the oceanic carbon cycle and the biological pump.

Data availability. Data is available at NOAA (https://www.ncdc.noaa.gov/paleo/study/30352, Guillermic et al., 2020).

Supplement. The supplement related to this article is available online at: https://doi.org/10.5194/bg-17-3487-2020-supplement.

Author contributions. RE and AT wrote the proposals that funded the work. AT and FC provided the samples. MG, SM, and AT contributed to the experimental design. AV helped for sample preparation. MG and SM contributed to developing the method of boron isotope analysis. MG performed the measurements with assistance from SM. MG conducted the data analysis. MG drafted the paper, which was edited by all authors. Interpretation was led by MG, AT, and SM with input from RE, AV, and FC.

Competing interests. The authors declare that they have no conflict of interest.

Acknowledgements. The authors wish to thank Jesse Farmer for his valuable and detailed comments on the current paper and a previous version of the paper. We wish to thank Michael Henehan for helpful discussion, comments on the manuscript, and help with the code. We also want to thank the anonymous reviewer for helpful comments. We thank Lea Bonnin for assistance with picking samples; the IODP repository for provision of samples; the Tripati Laboratory (UCLA) for their technical support; Mervyn Greaves and Madeleine Bohlin (University of Cambridge) for technical support and use of laboratory space; Yoan Germain, Emmanuel Ponzevera, and Oanez Lebeau for technical support and use of laboratory space in Brest; and Jill Sutton for helpful conversation about the manuscript. This research is supported by DOE BES grant DE-FG02-13ER16402, by the International Research Chair Program that is funded by the French government (LabexMer ANR-10-LABX-19-01), and IAGC student research grant 2017.

Financial support. This research has been supported by the DOE BES grant (grant no. DE-FG02-13ER16402), the LabexMer (grant no. ANR-10-LABX-19-01), and the IAGC (grant no. IAGC student grant 2017).

Review statement. This paper was edited by Markus Kienast and reviewed by Jesse Farmer, Michael Henehan, and one anonymous referee.

References

Allen, K. A. and Hönisch, B.: The planktic foraminiferal B/Ca proxy for seawater carbonate chemistry, A critical evaluation, Earth Planet. Sc. Lett., 345, 203–211, 2012.

Anagnostou, E., John, E., Edgar, K., Foster, G., Ridgwell, A., Inglis, G., Pancost, R., Lunt, D., and Pearson, P., Changing atmospheric CO_2 concentration was the primary driver of early Cenozoic climate, Nature, 533, 380–384, 2016.

Anand, P., Elderfield, H., and Conte, M. H., Calibration of Mg/Ca thermometry in planktonic foraminifera from a sediment trap time series, Paleoceanography, 18, 2003.

Anderson, O. R. and Bé, A.W. H.: The ultrastructure of a planktonic foraminifer, Globigerinoides sacculifer (Brady), and its symbiotic dinoflagellates, J. Foramin. Res., 6, 1–21, 1976.

Babila, T. L., Rosenthal, Y., and Conte, M. H.: Evaluation of the biogeochemical controls on B/Ca of Globigerinoides ruber white from the Oceanic Flux Pro-gram, Bermuda, Earth Planet. Sc. Lett., 404, 67–76, 2014.

Barker, S., Greaves, M., and Elderfield, H.: A study of cleaning procedures used for foraminiferal Mg/Ca paleothermometry, Geochem. Geophy. Geosy., 4, 1–20, 2003.

Bartoli, G., Hönisch, B., and Zeebe, R. E.: Atmospheric CO_2 decline during the Pliocene intensification of Northern Hemisphere glaciations, Paleoceanography 26, 1–14, 2011.

Bett, B. J.: RRS "Charles Darwin" Cruise 145, 12 March–9 April 2003, Benthic ecology and biogeochemistry of the Pakistan Margin (Southampton Oceanography Centre Cruise Report, 50) Southampton, UK, Southampton Oceanography Centre 161 pp., 2004.

Bijma, J., Hönisch, B., and Zeebe, R. E.: Impact of the ocean carbonate chemistry on living foraminiferal shell weight: Comment on "Carbonate ion concentration in glacial-age deep waters of the Caribbean Sea" by W. S. Broecker and E. Clark, Geochem. Geophy. Geosy., 3, 1–7, 2002.

Birch, H., Coxall, H. K., Pearson, P. N., Kroon, D., and O'Regan, M.: Planktonic foraminifera stable isotopes and water column structure, Disentangling ecological signals, Mar. Micropaleontol., 101, 127–145, 2013.

Bird, C., Darling, K. F., Russell, A. D., Fehrenbacher, J. S., Davis, C. V., Free, A., and Ngwenya, B. T.: 16S rRNA gene metabarcoding and TEM reveals different ecological strategies within the

genus Neogloboquadrina (planktonic foraminifer), PloS One, 13, 2018.

Black, K. S.: RRS Charles Darwin Cruise 107 cruise report, 1997.

Boyer, T. P., Antonov, J. I., Baranova, O. K., Coleman, C., Garcia, H. E., Grodsky, A., Johnson, D. R., Locarnini, R. A., Mishonov, A. V., O'Brien, T. D., Paver, C. R., Reagan, J. R., Seidov, D., Smolyar, I. V., and Zweng, M. M.: World Ocean Database 2013, Silver Spring, MD, NOAA Printing Officce, 208 pp. (NOAA Atlas NESDIS, 72), available at: http://hdl.handle.net/11329/357, 2013.

Boyle, E. A.: Cadmium, zinc, copper, and barium in foraminifera tests, Earth Planet. Sc. Lett., 53, 11–35, 1981.

Boyle, E. A. and Keigwin, L. D.: Comparison of Atlantic and Pacific paleochemical records for the Last 215,000 years: Changes in deep ocean circulation and chemical inventories, Earth Planet. Sc. Lett., 76, 135–150, 1985.

Catanzaro, E. J.: Boric acid: isotopic and assay standard reference materials (Vol. 260, No. 17), National Bureau of Standards, Institute for Materials Research, 1970.

Chalk, T. B., Hain, M. P., Foster, G. L., Rohling, E. J., Sexton, P. F., Badger, M. P. S., Cherry, S. G., Hasenfratz, A. P., Haug, G. H., Jaccard, S. L., Martínez-García, A., Pälike, H., Pancost, R. D., and Wilson, P. A.: Causes of ice age intensification across the Mid-Pleistocene Transition, P. Natl. Acad. Sci. USA, 114, 13114–13119, 2017.

Dekens, P. S., Lea, D. W., Pak, D. K., and Spero, H. J.: Core top calibration of Mg/Ca in tropical foraminifera, Refining paleotemperature estimation, Geochem. Geophy. Geosy., 3, 1–29, 2002.

de Nooijer, L. J., Spero, H. J., Erez, J., Bijma, J., and Reichart, G. J.: Biomineralization in perforate foraminifera, Earth-Sci. Rev., 135, 48–58, 2014.

Deuser, W. G. and Ross, E. H.: Seasonally abundant planktonic foraminifera of the Sargasso Sea, succession, deep-water fluxes, isotopic compositions, and paleoceanographic implications, J. Foramin. Res., 19, 268–293, 1989.

Deuser, W. G., Ross, E. H., Hemleben, C., and Spindler, M.: Seasonal changes in species composition, numbers, mass, size, and isotopic composition of planktonic foraminifera settling into the deep Sargasso Sea, Palaeogeogr., Palaeocl., 33, 103–127, 1981.

Dickson, A. G.: Thermodynamics of the dissociation of boric acid in synthetic seawater from 273.15 to 318.15 K, Deep-Sea Res. Pt. A, 37, 755–766, 1990.

Dickson, A. G. and Millero, F. J.: A comparison of the equilibrium constants for the dissociation of carbonic acid in seawater media, Deep-Sea Res., 34, 1733–1743, 1987.

Douville, E., Paterne, M., Cabioch, G., Louvat, P., Gaillardet, J., Juillet-Leclerc, A., and Ayliffe, L.: Abrupt sea surface pH change at the end of the Younger Dryas in the central sub-equatorial Pacific inferred from boron isotope abundance in corals (Porites), Biogeosciences, 7, 2445–2459, https://doi.org/10.5194/bg-7-2445-2010, 2010.

Duguay, L. E.: Comparative laboratory and field studies on calcification and carbon fixation in foraminiferal-algal associations, J. Foramin. Res., 13, 252–261, 1983.

Elderfield, H. and Granssen, G.: Past temperatures and δO^{18} of surface ocean waters inferred from foraminiferal Mg/Ca ratios, Nature, 405, 442–445, 2000.

Erez, J.: Calcification Rates, Photosynthesis and Light in Planktonic Foraminifera, in: Biomineralization and Biological Metal Accumulation, edited by: Westbroek, P. and de Jong, E. W., Springer, Dordrecht, 1983.

Erez, J.: The Source of Ions for Biomineralization in Foraminifera and Their Implications for Paleoceanographic Proxies, Rev. Mineral. Geochem., 54, 115–149, 2003.

Fairbanks, R. G. and Wiebe, P. H.: Foraminifera and Chlorophyll Maximum: Vertical Distribution, Seasonal Succession, and Paleoceanographic Significance, Science, 209, 1524–1526, 1980.

Fairbanks, R. G., Sverdlove, M., Free, R., Wiebe, P. H., and Bé, A. W. H.: Vertical distribution and isotopic fractionation of living planktonic foraminifera from the Panama Basin, Nature, 298, 841–844, 1982.

Farmer, E. C., Kaplan, A., de Menocal, P. B., and Lynch-Stieglitz, J.: Corroborating ecological depth preferences of planktonic foraminifera in the tropical Atlantic with the stable oxygen isotope ratios of core top specimens, Paleoceanography, 22, 1–14, 2007.

Farmer, J. R., Hönisch, B., and Uchikawa, J.: Single laboratory comparison of MC-ICP-MS and N-TIMS boron isotope analyses in marine carbonates, Chem. Geol., 447, 173–182, 2016.

Farmer, J. R., Branson, O., Uchikawa, J., Penman, D. E., Hönisch, B., and Zeebe, R. E.: Boric acid and borate incorporation in inorganic calcite inferred from B/Ca, boron isotopes and surface kinetic modeling, Geochim. Cosmochim. Ac., 244, 229–247, 2019.

Foster, G. L.: Seawater pH, pCO_2 and $[CO_3^{2-}]$ variations in the Caribbean Sea over the last 130 kyr: A boron isotope and B/Ca study of planktic foraminifera, Earth Planet. Sc. Lett., 271, 254–266, 2008.

Foster, G. L. and Rae, J. W. B.: Reconstructing Ocean pH with Boron Isotopes in Foraminifera, Annu. Rev. Earth Pl. Sc., 44, 207–237, 2016.

Foster, G. L. and Sexton, P. F.: Enhanced carbon dioxide outgassing from the eastern equatorial Atlantic during the last glacial, Geology, 42, 1003–1006, 2014.

Foster, G. L., Pogge von Strandmann, P. A., and Rae, J. W. B.: Boron and magnesium isotopic composition of seawater, Geochem. Geophy. Geosy., 11, Q08015, https://doi.org/10.1029/2010GC003201, 2010.

Foster, G. L., Lear, C. H., and Rae, J. W. B.: The evolution of pCO_2, ice volume and climate during the middle Miocene, Earth Planet. Sc. Lett., 341, 243–254, 2012.

Gabitov, R. I., Rollion-bard, C., Tripati, A., and Sadekov, A.: In situ study of boron partitioning between calcite and fluid at different crystal growth rates, Geochim. Cosmochim. Ac., 137, 81–92, 2014.

Gaillardet, J., Lemarchand, D., Göpel, C., and Manhès, G.: Evaporation and Sublimation of Boric Acid?: Application for Boron Purification from Organic Rich Solutions, Geostand. Newsl., 25, 67–75, 2001.

Gast, R. J. and Caron D. A.: Photosymbiotic associations in planktonic foraminifera and radiolaria, Hydrobiologia, 461, 1–7, 2001.

Gastrich, M. D.: Ultrastructure of a new intracellular symbiotic alga found within planktonic foraminifera, J. Phycol., 23, 623–632, 1988.

Guillermic, M., Misra, S., Eagle, R. A., Villa, A., Chang, F., and Tripati, A. K.: Global Ocean Planktonic Foraminifera Boron Isotope Seawater pH Reconstruction, available at: https://www.ncdc.noaa.gov/paleo/study/30352, last access: 7 July 2020.

Gutjahr, M., Bordier, L., Douville, E., Farmer, J., Foster, G. L., Hathorne, E., Hönish, B., Lemarchand, D., Louvat, P., McCulloch, M., Noireaux, J., Pallavicini, N., Rodushkin, I., Roux, P., Stewart, J., Thil, F., and You, C. F.: Boron Isotope Intercomparison Project (BIIP): Development of a new carbonate standard for stable isotopic analyses, In EGU general assembly conference abstracts (Vol. 16), May 2014.

Hallock P.: Algal Symbiosis?: A mathematical analysis, Mar. Biol., 62, 249–255, 1981.

Hendry, K. R., Rickaby, R. E. M., Meredith, M. P., and Elderfield, H.: Controls on sta-ble isotope and trace metal uptake in Neogloboquadrina pachyderma (sinis-tral) from an Antarctic sea-ice environment, Earth Planet. Sc. Lett., 278, 67–77, 2009.

Henehan, M. J., Rae, J. W. B., Foster, G. L., Erez, J., Prentice, K. C., Kucera, M., Bostock, H. C., Martínez-Botí, M. A., Milton, J. A., Wilson, P. A., Marshall, B. J., and Elliott, T.: Calibration of the boron isotope proxy in the planktonic foraminifera Globigerinoides ruber for use in palaeo-CO_2 reconstruction, Earth Planet. Sc. Lett. 364, 111–122, 2013.

Henehan, M. J., Foster, G. L., Rae, J. W. B., Prentice, K. C., Erez, J., Bostock, H. C., Marshall, B. J., and Wilson, P. A.: Evaluating the utility of B/Ca ratios in planktic foraminifera as a proxy for the carbonate system: A case study of Globigerinoides ruber, Geochem. Geophy. Geosy., 16, 1052–1069, 2015.

Henehan, M. J., Foster, G. L., Bostock, H. C., Greenop, R., Marshall, B. J., and Wilson, P. A.: A new boron isotope-pH calibration for Orbulina universa, with implications for understanding and accounting for "vital effects", Earth Planet. Sc. Lett., 454, 282–292, 2016.

Holcomb, M., Decarlo, T. M., Schoepf, V., Dissard, D., Tanaka, K., and McCulloch, M.: Cleaning and pre-treatment procedures for biogenic and synthetic calcium carbonate powders for determination of elemental and boron isotopic compositions, Chem. Geol., 398, 11–21, 2015.

Hönisch, B. and Hemming, N. G.: Ground-truthing the boron isotope-paleo-pH proxy in planktonic foraminifera shells: Partial dissolution and shell size effects, Paleoceanography 19, 1–13, 2004.

Hönisch, B. and Hemming, N. G.: Surface ocean pH response to variations in pCO_2 through two full glacial cycles, Earth Planet. Sc. Lett., 236, 305–314, 2005.

Hönisch, B., Bijma, J., Russell, A. D., Spero, H. J., Palmer, M. R., Zeebe, R. E., and Eisenhauer, A.: The influence of symbiont photosynthesis on the boron isotopic composition of foraminifera shells, Mar. Micropaleontol., 49, 87–96, 2003.

Hönisch, B., Hemming, N. G., Archer, D., Siddall, M., and McManus, J. F.: Atmospheric Carbon Dioxide Concentration Across the Mid-Pleistocene Transition, Science, 324, 1551–1554, 2009.

Howes, E. L., Kaczmarek, K., Raitzsch, M., Mewes, A., Bijma, N., Horn, I., Misra, S., Gattuso, J.-P., and Bijma, J.: Decoupled carbonate chemistry controls on the incorporation of boron into Orbulina universa, Biogeosciences, 14, 415–430, https://doi.org/10.5194/bg-14-415-2017, 2017.

IPCC: Climate Change 2014 – The Physical Science Basis, edited by Intergovernmental Panel on Climate Change, Cambridge University Press, Cambridge, 2014.

Jørgensen, B. B., Erez, J., Revsbech, P., and Cohen, Y.: Symbiotic photosynthesis in a planktonic foraminifera, Globigerinoides sacculifer (Brady), studied with microelectrodes, Limnol. Oceanogr., 30, 1253–1267 1985.

Kaczmarek, K., Nehrke, G., Misra, S., Bijma, J., and Elderfield, H.: Investigating the effects of growth rate and temperature on the B/Ca ratio and $\delta^{11}B$ during inorganic calcite formation, Chem. Geol., 421, 81–92, 2016.

Kemle-von Mücke, S. and Oberhänsli, H.: The distribution of living planktic foraminifera in relation to southeast Atlantic oceanography, in: Use of proxies in paleoceanography, Springer, Berlin, Heidelberg, 91–115, 1999.

Key, R. M.: A global ocean carbon climatology: Results from Global Data Analysis Project (GLODAP), Global Biogeochem. Cy., 18, GB4031, https://doi.org/10.1029/2004GB002247, 2004.

Klochko, K., Kaufman, A. J., Yao, W., Byrne, R. H., and Tossell, J. A.: Experimental measurement of boron isotope fractionation in seawater, Earth Planet. Sc. Lett., 248, 276–285, 2006.

Köhler-Rink, S. and Kühl, M.: Microsensor studies of photosynthesis and respiration in larger symbiotic foraminifera. I. The physico-chemical microenvironment of Marginopora vertebralis, Amphistegina lobifera and Amphisorus hemrichii, Mar. Biol., 137, 473–486, 2000.

Lea, D. W., Pak, D. K., and Spero, H. J.: Climate impact of late quaternary equatorial Pacific sea surface temperature variations, Science, 289, 1719–1724, 2000.

Lee, K., Kim, T. W., Byrne, R. H., Millero, F. J., Feely, R. A., and Liu, Y. M.: The universal ratio of boron to chlorinity for the North Pacific and North Atlantic oceans, Geochim. Cosmochim. Ac., 74, 1801–1811, 2010.

Lemarchand, D., Gaillardet, J., Lewin, A., and Allègre, C. J.: Boron isotope systematics in large rivers: Implications for the marine boron budget and paleo-pH reconstruction over the Cenozoic, Chem. Geol., 190, 123–140, 2002.

Liu, Y., Liu, W., Peng, Z., Xiao, Y., Wei, G., Sun, W., He, J., Liu, G., and Chou, C. L.: Instability of seawater pH in the South China Sea during the mid-late Holocene: Evidence from boron isotopic composition of corals, Geochim. Cosmochim. Ac., 73, 1264–1272, 2009.

Lloyd, N. S., Sadekov, A. Y., and Misra, S.: Application of 10^{13} ohm Faraday cup current amplifiers for boron isotopic analyses by solution mode and laser ablation multicollector inductively coupled plasma mass spectrometry, Rapid Commun. Mass Spec., 32, 9–18, 2018.

Marschall, H. and Foster, G.: Boron Isotopes, the fifth element, Advances in Isotope Geochemistry, https://doi.org/10.1007/978-3-319-64666-4, 2018.

Martínez-Botí, M. A., Foster, G. L., Chalk, T. B., Rohling, E. J., Sexton, P. F., Lunt, D. J., Pancost, R. D., Badger, M. P. S., and Schmidt, D. N.: Plio-Pleistocene climate sensitivity evaluated using high-resolution CO_2 records, Nature, 518, 49–54, 2015a.

Martínez-Botí M. A., Marino G., Foster G. L., Ziveri P., Henehan M. J., Rae J. W. B., Mortyn P. G., and Vance D.: Boron isotope evidence for oceanic carbon dioxide leakage during the last deglaciation, Nature, 518, 219–222, 2015b.

Mavromatis, V., Montouillout, V., Noireaux, J., Gaillardet, J., and Schott, J.: Characterization of boron incorporation and speciation in calcite and aragonite from co-precipitation experiments under controlled pH, temperature and precipitation rate, Geochim. Cosmochim. Ac., 150, 299–313, 2015.

McCulloch, M. T., D'Olivo, J. P., Falter, J., Georgiou, L., Holcomb, M., Montagna, P., and Trotter, J. A.: Boron isotopic systematics in scleractinian corals and the role of pH up-regulation, in: Boron Isotopes, Springer, Chamber, 145–162, 2018.

Mehrbach, C., Culberson, C. H., Hawley, J. E., and Pytkowicx, R. M.: Measurement of the apparent dissociation constants of carbonic acid in seawater at atmospheric pressure 1, Limnol. Oceanogr., 18, 897–907, 1973.

Misra, S., Greaves, M., Owen, R., Kerr, J., Elmore, A. C., and Elderfield, H.: Determination of B/Ca of natural carbonates by HR-ICP-MS, Geochem. Geophy. Geosy., 15, 1617–1628, 2014a.

Misra, S., Owen, R., Kerr, J., Greaves, M., and Elderfield, H.: Determination of δ^{11}B by HR-ICP-MS from mass limited samples: Application to natural carbonates and water samples, Geochim. Cosmochim. Ac., 140, 531–552, 2014b.

Mortyn, P. G. and Charles, C. D.: Planktonic foraminiferal depth habitat and δ^{18}O calibrations: Plankton tow results from the Atlantic sector of the Southern Ocean, Paleoceanography, 18, 1037, https://doi.org/10.1029/2001PA000637, 2003.

Ni, Y., Foster, G. L., Bailey, T., Elliott, T., Schmidt, D. N., Pearson, P., Haley, B., and Coath, C.: A core top assessment of proxies for the ocean carbonate system in surface-dwelling foraminifers, Paleoceanography, 22, PA3212, https://doi.org/10.1029/2006PA001337, 2007.

Nir, O., Vengosh, A., Harkness, J. S., Dwyer, G. S., and Lahav, O.: Direct measurement of the boron isotope fractionation factor: Reducing the uncertainty in reconstructing ocean paleo-pH, Earth Planet. Sc. Lett., 414, 1–5, 2015.

Pagani, M.: Marked Decline in Atmospheric Carbon Dioxide Concentrations During the Paleogene, Science, 309, 600–603, 2005.

Palmer, M. R., Pearson, P. N., and Cobb, S. J.: Reconstructing Past Ocean pH-Depth Profiles, Science, 282, 1468–1471, 1998.

Pearson, P. N. and Palmer, M. R.: Middle Eocene seawater pH and atmospheric carbon dioxide concentrations, Science, 284, 1824–1826, 1999.

Quintana Krupinski, N. B., Russell, A. D., Pak, D. K., and Paytan, A.: Core-top calibration of B/Ca in Pacific Ocean Neogloboquadrina incompta and Globigerina bulloides as a surface water carbonate system proxy, Earth Planet. Sc. Lett., 466, 139–151, 2017.

Rae, J. W. B.: Boron Isotopes in Foraminifera: Systematics, Biomineralisation, and CO_2 Reconstruction, in: Boron Isotopes, Advances in Isotope Geochemistry, edited by: Marschall, H. and Foster, G., Springer, Cham, 2018.

Rae, J. W. B., Foster, G. L., Schmidt, D. N., and Elliott, T.: Boron isotopes and B/Ca in benthic foraminifera: Proxies for the deep ocean carbonate system, Earth Planet. Sc. Lett., 302, 403–413, 2011.

Raitzsch, M., Bijma, J., Benthien, A., Richter, K.-U., Steinhoefel, G., and Kučera, M.: Boron isotope-based seasonal paleo-pH reconstruction for the Southeast Atlantic – A multispecies approach using habitat preference of planktonic foraminifera, Earth Planet. Sc. Lett., 487, 138–150, 2018.

Ravelo, A. C. and Fairbanks, R. G.: Oxygen isotopic composition of multiple species of planktonic foraminifera: recorder of the modern photic zone temperature gradient, Palaeogeogr. Palaeocl., 7, 815–831, 1992.

Rebotim, A., Voelker, A. H. L., Jonkers, L., Waniek, J. J., Meggers, H., Schiebel, R., Fraile, I., Schulz, M., and Kucera, M.: Factors controlling the depth habitat of planktonic foraminifera in the subtropical eastern North Atlantic, Biogeosciences, 14, 827–859, https://doi.org/10.5194/bg-14-827-2017, 2017.

Regenberg, M., Steph, S., Nürnberg, D., Tiedemann, R., and Garbe-Schönberg, D.: Calibrating Mg/Ca ratios of multiple planktonic foraminiferal species with δ^{18}O-calcification temperatures, Paleothermometry for the upper water column, Earth Planet. Sc. Lett., 278, 324–336, 2009.

Rickaby, R. E. M. and Halloran, P.: Cool La Nina During the Warmth of the Pliocene?, Science, 307, 1948–1952, 2005.

Ries, J. B., Cohen, A. L., and McCorkle, D. C.: Marine calcifiers exhibit mixed responses to CO_2-induced ocean acidification, Geology, 37, 1131–1134, 2009.

Rink, S., Kühl, M., Bijma, J., and Spero, H. J.: Microsensor studies of photosynthesis and respiration in the symbiotic foraminifer Orbulina universa, Mar. Biol., 131, 583–595, 1998.

Rollion-Bard, C. and Erez, J.: Intra-shell boron isotope ratios in the symbiont-bearing benthic foraminiferan Amphistegina lobifera: Implications for δ^{11}B vital effects and paleo-pH reconstructions, Geochim. Cosmochim. Ac., 74, 1530–1536, 2010.

Sanyal, A., Hemming, N. G., Broecker, W. S., Lea, D. W., Spero, H. J., and Hanson, G. N.: Oceanic pH control on the boron isotopic composition of foraminifera: evidence from culture experiments, Paleoceanography, 11, 513–517, 1996.

Sanyal, A., Bijma, J., Spero, H. J., and Lea, D. W.: Empirical relationship between pH and the boron isotopic composition of Globigerinoides sacculifer: Implications for the boron isotopes paleo-pH proxy, Paleoceanography, 16, 515–519, 2001.

Schmidt, G. A. and Mulitza, S.: Global calibration of ecological models for planktic foraminifera from core-top carbonate oxygen-18, Mar. Micropaleontol., 44, 125–140, 2002.

Seki, O., Foster, G. L., Schmidt, D. N., Mackensen, A., Kawamura, K., and Pancost, R. D.: Alkenone and boron-based Pliocene pCO2records, Earth Planet. Sc. Lett., 292, 201–211, 2010.

Shaked, Y. and de Vargas, C.: Pelagic photosymbiosis: rDNA assessment of diversity and evolution of dinoflagellate symbionts and planktonic foraminiferal hosts, Mar. Ecol. Prog. Ser., 325, 59–71, 2006.

Sime, N. G., De La Rocha, C. L., and Galy, A.: Negligible temperature dependence of calcium isotope fractionation in 12 species of planktonic foraminifera, Earth Planet. Sc. Lett., 232, 51–66, 2005.

Spero, H. J.: Symbiosis in the planktonic foraminifer, orbulina universa, and the isolation of its symbiotic dinoflagellate, gymnodinium beii sp.nov, J. Phycol., 23, 307–317, 1987.

Steinhardt, J., de Nooijer, L. L., Brummer, G. J., and Reichart, G. J.: Profiling planktonic foraminiferal crust formation, Geochem. Geophy. Geosy., 16, 2409–2430, 2015.

Sutton, J. N., Liu, Y.-W., Ries, J. B., Guillermic, M., Ponzevera, E., and Eagle, R. A.: δ^{11}B as monitor of calcification site pH in divergent marine calcifying organisms, Biogeosciences, 15, 1447–1467, https://doi.org/10.5194/bg-15-1447-2018, 2018.

Takagi, H., Kimoto, K., Fujiki, T., Saito, H., Schmidt, C., Kucera, M., and Moriya, K.: Characterizing photosymbiosis in modern planktonic foraminifera, Biogeosciences, 16, 3377–3396, https://doi.org/10.5194/bg-16-3377-2019, 2019.

Thomson, J., Brown, L., Nixon, S., Cook, G. T., and MacKenzie, A. B.: Bioturbation and Holocene sediment accumulation fluxes in

the north-east Atlantic Ocean (Benthic Boundary Layer experiment sites), Mar. Geol., 169, 21–39, 2000.

Tripati, A. K., Roberts, C. D., and Eagle, R. A.: Coupling of CO_2 and Ice Sheet Stability Over Major Climate Transitions of the Last 20 Million Years, Science, 326, 1394–1397, 2009.

Tripati, A. K., Roberts, C. D., Eagle, R. A., and Li, G.: A 20 million year record of planktic foraminiferal B/Ca ratios: Systematics and uncertainties in pCO_2 reconstructions, Geochim. Cosmochim. Ac., 75, 2582–2610, 2011.

Uchikawa, J., Penman, D. E., Zachos, J. C., and Zeebe, R. E.: Experimental evidence for kinetic effects on B/Ca in synthetic calcite: Implications for potential $B(OH)_4^-$ and $B(OH)_3$ incorporation, Geochim. Cosmochim. Ac., 150, 171–191, 2015.

Urey, H. C., Lowenstam, H. A., Epstein, S., and McKinney, C. R.: Measurement of paleo-temperature and temperatures of the upper cretaceous of England, Denmark, and the southeastern United-States, Geol. Soc. Am. Bull., 62, 399–416, 1951.

Vogl, J. and Rosner, M.: Production and certification of a unique set of isotope and delta reference materials for boron isotope determination in geochemical, environmental and industrial materials, Geostand. Geoanal. Res., 36, 161–175, 2011.

Wang, B.-S., You, C.-F., Huang, K.-F., Wu, S.-F., Aggarwal, S. K., Chung, C.-H., and Lin, P.-Y.: Direct separation of boron from Na- and Ca-rich matrices by sublimation for stable isotope measurement by MC-ICP-MS, Talanta, 82, 1378–1384, 2010.

Wang, G., Cao, W., Yang, D., and Xu, D.: Variation in downwelling diffuse attenuation coefficient in the northern South China Sea, Chinese J. Oceanol. Limnol., 26, 323–333, 2008.

Weare, B. C., Strub, P. T., and Samuel, M. D.: Annual Mean Surface Heat Fluxes in the Tropical Pacific Ocean, J. Phys. Oceanogr., 11, 705–717, 1981.

Wei, G., McCulloch, M. T., Mortimer, G., Deng, W., and Xie, L.: Evidence for ocean acidification in the Great Barrier Reef of Australia, Geochim. Cosmochim. Ac., 73, 2332–2346, 2009.

Wilson, D. J., Piotrowski, A. M., Galy, A., and McCave, I. N.: A boundary exchange influence on deglacial neodymium isotope records from the deep western Indian Ocean, Earth Planet. Sc. Lett., 341, 35–47, 2012.

Wolf-Gladrow, D. A., Riebesell, U., Burkhardt, S., and Buma, J.: Direct effects of CO_2 concentration on growth and isotopic composition of marine plankton, Tellus B, 51, 461–476, 1999.

Yu, J., Elderfield, H., and Hönisch, B.: B/Ca in planktonic foraminifera as a proxy for surface seawater pH, Paleoceanography, 22, PA2202, https://doi.org/10.1029/2006PA001347, 2007.

Yu, J., Foster, G. L., Elderfield, H., Broecker, W. S., and Clark, E.: An evaluation of benthic foraminiferal B/Ca and $\delta^{11}B$ for deep ocean carbonate ion and pH reconstructions, Earth Planet. Sc. Lett., 293, 114–120, 2010.

Yu, J., Thornalley, D. J. R., Rae, J. W. B., and McCave, N. I.: Calibration and application of B/Ca, Cd/Ca, and $\delta^{11}B$ in Neogloboquadrina pachyderma (sinistral) to constrain CO_2 uptake in the subpolar North Atlantic during the last deglaciation, Paleoceanography, 28, 237–252, 2013.

Yu, J., Menviel, L., Jin, Z. D., Thornalley, D. J. R., Barker, S., Marino, G., Rohling, E. J., Cai, Y., Zhang, F., Wang, X., Dai, Y., Chen, P., and Broecker, W. S.: Sequestration of carbon in the deep Atlantic during the last glaciation, Nat. Geosci., 9, 319–324, 2016.

Zeebe, R. E. and Wolf-Gladrow, D.: CO_2 in Seawater: Equilibrium, Kinetics, Isotopes Elsevier Oceanography Series, No. 65, Gulf Professional Publishing, Amsterdam, 2001.

Zeebe, R. E., Wolf-Gladrow, D. A., Bijma, J., and Hönisch, B.: Vital effects in foraminifera do not compromise the use of $\delta^{11}B$ as a paleo-pH indicator: Evidence from modeling, Paleoceanography, 18, 1043, https://doi.org/10.1029/2003PA000881, 2003.